

Structural determinants in the C-terminal  
cytoplasmic region for the slow deactivation  
of hERG K<sup>+</sup> channel

Kume, Shinichiro

Doctor of Philosophy

Department of Physiological Sciences

School of Life Science

SOKENDAI (The Graduate University for  
Advanced Studies)



Structural determinants in the C-terminal cytoplasmic region  
for the slow deactivation of hERG K<sup>+</sup> channel

Kume, Shinichiro

SOKENDAI (The Graduate University for Advanced Studies)

School of Life Science

Department of Physiological Sciences

## **Contents**

Abstract	1
Introduction	4
Materials & Methods	10
Results	15
Discussion	22
References	30
Figure legends	37
Table	51
Figure	52
Acknowledgements	74

## Abstract

Human Ether-a-go-go Related Gene (hERG) channel, which belongs to the voltage-gated  $K^+$  channel (Kv) family, is well known for its very slow deactivation kinetics. This slow deactivation is important for the repolarization of cardiac action potential in myocytes, and is known to be regulated by its intracellular regions.

In the C-terminal intracellular region, members in the KCNH subfamily including hERG channel have Cyclic Nucleotide Binding (CNB) domain which is connected to the sixth transmembrane helix by C-linker domain. Although the binding of cyclic nucleotides to the ligand binding pocket of CNB domain regulates the channel gating in Hyperpolarization-activated Cyclic Nucleotide-modulated (HCN) and Cyclic Nucleotide-Gated (CNG) channels, KCNH channels are known to lack the sensitivity to cyclic nucleotides. In hERG channel, several mutations and truncation of C-linker or CNB domains show accelerated deactivation kinetics, suggesting that the roles of these domains of hERG channel differ from those of HCN and CNG channels. It remains unknown, however, how these domains control the slow deactivation of hERG channel.

The crystal structures of C-linker and CNB domains of two KCNH channels, zebrafish Ether-a-go-go Like K<sup>+</sup> (zELK) and Anopheles gambiae ERG (agERG) channels, were solved recently. These studies suggest that the structures of them basically resemble one another, but have some differences from that of mHCN2 channel. To obtain the structural insight of C-linker and CNB domains of hERG channel, I performed the structure homology modeling of these domains of hERG channel

based on those of agERG channel.

The homology model of hERG channel showed that a side chain of an amino acid residue Phe860 occupied the ligand binding pocket as if Phe860 is an endogenous ligand. This may explain the lack of sensitivity to cyclic nucleotides. It was also indicated that there are two electrostatic interactions between C-linker and CNB domains in hERG channel, similarly to HCN and CNG channels. The two interactions are possibly formed between Arg696 in C-linker domain and Asp767 in CNB domain, and Arg696 and Asp727 in C-linker domain, respectively. In this study, I aimed at elucidation of the role of Phe860 in the gating, and functional conformation of the existence of the two electrostatic interactions between C-linker and CNB domains. I analyzed the functional electrophysiological properties of various mutants by two electrode voltage clamp technique using *Xenopus* oocytes.

The substitution of Phe860 with charged Arg or Glu accelerated the deactivation kinetics, but that with hydrophobic Ile or Val did not change the kinetics. In addition, the substitution to small hydrophobic Ala also accelerated the deactivation. These results indicate that the hydrophobicity and bulkiness of the amino acid side chain are necessary to maintain the slow deactivation in this position, and that Phe860 occupies the ligand binding pocket to play an important role to control the slow deactivation in hERG channel, unlike the mechanisms of HCN and CNG channels.

Next, I investigated two electrostatic interactions in C-linker and CNB domains. The mutant of Arg696 to Glu showed slower deactivation kinetics than wild type (WT). In contrast, when Asp767 or Asp727 was substituted with Lys, both mutants accelerated the deactivation. Their different phenotypes

suggest that there is no direct electrostatic interaction between Arg696 and Asp767, and Arg696 and Asp727, unlike the case of HCN and CNG channels. However, only the double mutant of Arg696Glu and Asp767Lys showed much slower deactivation kinetics than WT and each single mutant. The results suggest that Arg696 and Asp767 are not independent and have indirect but functional interaction.

Regarding Asp727 which was shown not to be the counterpart for Arg696, I identified a novel direct electrostatic interaction by systematic mutagenesis. When I substituted Arg752 in CNB domain to Glu, this mutant showed accelerated deactivation kinetics like Asp727Lys. Furthermore, the double mutant of Asp727Lys and Arg752Glu recovered the slow deactivation kinetics to the same degree of WT. These results suggest that Asp727 directly interacts with Arg752 electrostatically to maintain the slow deactivation. As a positively charged amino acid at 752 is conserved only in KCNH subfamily, but not in HCN and CNG channels, it is thought that this interaction is a unique one of KCNH family members.

Taken together, I found that the C-linker and CNB domains of hERG channel contribute to the control of slow deactivation by different mechanisms from those of HCN and CNG channels, such as the endogenous ligand like role of Phe860 and the novel electrostatic interaction between Asp727 and Arg752. As some amino acids residues related to these mechanisms were reported as a cause of the cardiac diseases such as LQT2, it is thought that the results in this study would contribute to elucidate the mechanisms of these diseases.

## Introduction

The voltage-gated K<sup>+</sup> channels (Kv) are the largest family among ion channels, which sense the membrane potential change to open and close the channel gate and conduct K<sup>+</sup> ion selectively. Human Ether-a-go-go Related Gene (hERG) channel belonging to Kv family is well known to play an important role for repolarization phase of the action potential in cardiac myocytes. It is known a malfunction of hERG channel by drug application or by its inherited mutation cause long QT syndrome which is associated with a risk of ventricular arrhythmias and sudden death (Curran *et al.*, 1995; January *et al.*, 2000; Roden, 2006; Sanguinetti & Tristani-Firouzi, 2006; Shimizu, 2008; Sanguinetti, 2010; Foo *et al.*, 2016).

One of the characteristic features of hERG channel function is far slower deactivation than those of other Kvs (Sanguinetti *et al.*, 1995; Trudeau *et al.*, 1995). Deactivation is the process in which the open channel returns to the resting state upon hyperpolarization, and the slow deactivation of hERG channel is known to be controlled by the intracellular regions (Gustina & Trudeau, 2012; Vandenberg *et al.*, 2012; Morais-Cabral & Robertson, 2015; Perry *et al.*, 2015).

Each subunit of Kv has six transmembrane segments and four subunits assemble to form a functioning unit (Sands *et al.*, 2005; Tombola *et al.*, 2006). Among these six transmembrane segments (S1-S6), the former four (S1-S4) function as the voltage sensor domain (Smith & Yellen, 2002; Zhang *et al.*, 2004; Piper *et al.*, 2005; Cheng & Claydon, 2012) (Figure 1A). The latter two (S5-S6) form the channel pore domain (Wynia-Smith *et al.*, 2008; Thouta *et al.*, 2014). The pore domains of four subunits

assemble in the center of the channel structure, and the voltage sensor domains are located surrounding them. The basic structure of hERG channel is similar to other Kvs. However, the intracellular regions of the hERG channel are much larger than other Kvs. All the three intracellular regions, N-terminal, S4-S5 linker and C-terminal, are known to be critical for slow deactivation (Warmke & Ganetzky, 1994; Gustina & Trudeau, 2012; Vandenberg *et al.*, 2012; Morais-Cabral & Robertson, 2015) (Figure 1A).

N-terminal region of hERG channel contains the Ether-a-go-go (EAG) domain (1-135 amino acids), which consists of N-tail domain (1-25 amino acids) and Per-Arn-Sim (PAS) domain (26-135 amino acids) (Morais Cabral *et al.*, 1998) (Figure 1A). EAG domain is conserved well among KCNH subfamily including hERG channel (Warmke & Ganetzky, 1994). Former studies of hERG channel showed that the truncation of EAG domain (Sanguinetti *et al.*, 1995; Trudeau *et al.*, 1995; Schonherr & Heinemann, 1996; Spector *et al.*, 1996; Wang *et al.*, 2000) and as well as mutations in EAG domain (Morais Cabral *et al.*, 1998; Chen *et al.*, 1999; Muskett *et al.*, 2011; Ng *et al.*, 2011; Gianulis & Trudeau, 2011; Tan *et al.*, 2012; Ke *et al.*, 2013) accelerated the slow deactivation. When the N-terminal truncation mutant of hERG channel ( $\Delta 2-354$ ) or a splice variant which lacks most of the N-terminal region was co-expressed with the EAG domain protein (1-135), the deactivation was restored (Gustina & Trudeau, 2009; Trudeau *et al.*, 2011). However, the slow deactivation of truncation mutant of hERG channel which lacks both N- and C-terminal cytoplasmic regions ( $\Delta 2-354$ ,  $\Delta 749-1159$ ) was not restored by coexpression with the EAG domain (Gustina & Trudeau, 2011), suggesting that the EAG domain interacts with C-terminal region to control the deactivation. Furthermore, it was shown that EAG

domain interacts with S4-S5 linker domain which connects voltage sensing domain and pore domain (de la pena *et al.*, 2011; de la pena *et al.*, 2013; de la pena *et al.*, 2014). Mutations in S4-S5 linker domain also affected the deactivation kinetics (Sanguinetti & Xu, 1999; Van Slyke *et al.*, 2010; Ng *et al.*, 2012; Hull *et al.*, 2014).

In the C-terminal intracellular region of hERG channel, there is a cyclic nucleotide binding (CNB) domain (Warmke & Ganetzky, 1994) (Figures 1, 2). This domain is connected to the pore forming domain by C-linker domain (Figures 1, 2). A truncation and mutations of these domains were shown to change the deactivation speed (Ficker *et al.*, 2000; Aydar & Palmer, 2001; Al-Owais *et al.*, 2009; Muskett *et al.*, 2011; Gustina & Trudeau, 2013; Ng *et al.*, 2014). It has been also reported that C-linker and CNB domain interact with EAG domain to control the slow deactivation (Gustina & Trudeau, 2011; Fernandez-Trillo *et al.*, 2011; Gustina & Trudeau, 2013; Haitin *et al.*, 2013; Ng *et al.*, 2014).

The structure of C-linker and CNB domains has been solved in mouse Hyperpolarization-activated Cyclic Nucleotide-modulated 2 (mHCN2) channel belonging Kv family (Zagotta *et al.*, 2003). Thereafter, the structures have been solved in SplH, MloK1, hHCN4 and SthK channels which are closely related to the mHCN2 channel (Flynn *et al.*, 2007; Schunke *et al.*, 2009; Schunke *et al.*, 2011; Akimoto *et al.*, 2014; Kesters *et al.*, 2015). These results suggested that C-linker and the CNB domains assembled in a tetramer.

CNB domain is conserved in HCN and Cyclic Nucleotide-Gated (CNG) channels, and KCNH

subfamily including hERG channel (Figures 2, 3A). HCN channel is a voltage gated channel which opens upon hyperpolarization. In HCN channel, the binding of cyclic nucleotide (cAMP) to the ligand binding pocket shifts the voltage dependence to depolarized potential (Craven & Zagotta, 2006; Wahl-Schott & Biel, 2009). Therefore, the channel can open at less hyperpolarized membrane potential. In contrast, CNG channel has no voltage dependence and opens simply by cyclic nucleotide (cGMP) binding (Kaupp & Seifert, 2002; Craven & Zagotta, 2006). In both channels, it has been suggested that the binding of cyclic nucleotide changed the structure of CNB domain, which is transmitted to the C-linker domain using inter-domain interaction to control the gating (Johnson & Zagotta., 2001; Zagotta *et al.*, 2003; Hua & Gordon, 2005). In HCN channel, it is known that there are interactions between Lys472 in C-linker domain and Glu502 in neighbor subunit's C-linker domain, and between Lys472 and Asp542 in CNB domain of same subunit (Craven & Zagotta, 2004) (Figures 1B, 2). In addition, same interactions are known also in CNG channel (Craven & Zagotta, 2004; Craven *et al.*, 2008).

KCNH subfamily members including hERG channel do not have a sensitivity to cyclic nucleotide unlike HCN and CNG channels (Frings *et al.*, 1998; Brelidze *et al.*, 2009) (Figure 3A). Therefore, it was unclear whether or not C-linker and CNB domains of KCNH subfamily have a similar structural determinant found in HCN and CNG channels for many years. However, the crystal structure of these C-terminal domains was solved in zebrafish Ether-a-go-go Like K<sup>+</sup> (zELK) channel belonging to KCNH subfamily (Brelidze *et al.*, 2012). The results suggested that the structure of zELK resembled mHCN2 channel, but with some interesting differences. In zELK channel, a side chain of the amino acid

residue Tyr740 filled the ligand binding pocket as if as an endogenous ligand, explaining the lack of sensitivity to cyclic nucleotide. Furthermore, the structure of zELK channel was in an unnatural dimer form probably due to crystallization artifact. More recently, the structure of these C-terminal domains of *Anopheles gambiae* ERG (agERG) and zebrafish KCNH channels were also solved in a monomeric state (Brelidze *et al.*, 2013; Li *et al.*, 2014), and those of mouse EAG (mEAG) channel were also solved as the complex with EAG domain (Haitin *et al.*, 2013). These crystal structures showed overall a similar structure to that of zELK channel. The information as to the manner of inter-subunit interaction in KCNH family was not given by these studies. Also the structure of hERG channel itself remains to be solved till now.

Thus, the importance of the charged interactions between C-linker and CNB domains clearly observed in HCN channel has not been analyzed in hERG channel until now. Therefore, I performed the structure homology modeling for C-linker and CNB domains of hERG channel based on the structure of monomeric agERG channel towards the understanding of structural determinants of C-linker and CNB domains. In this study, I analyzed the role of Phe860 which corresponds to Tyr740 in zELK channel in the gating of hERG channel. Next, I analyzed similarities and differences of the interaction between C-linker and CNG domains of hERG channel to those of HCN and CNG channels.

I revealed Phe860, a bulky hydrophobic amino acid, fills the ligand binding pocket to control the slow deactivation. In addition, among the interacting amino acid pairs between C-linker and CNB domains, Arg696 and Asp767 were shown to interact functionally. Furthermore, I newly found a direct

interaction, critical for slow deactivation, between Asp727 and Arg752 in CNB domain, which is not observed in HCN and CNG channels.

## Materials and Methods

### Homology modeling

The homology structure modeling of the C-linker domain between 666 and 747 amino acid residues and cyclic nucleotide binding (CNB) domain between 748 and 872 amino acid residues of human ERG1a (hERG1a) channel were performed using SWISS-MODEL server (<http://swissmodel.expasy.org>) based on the monomeric crystal structure of *Anopheles gambiae* ERG channel (PDB: 4L11).

### Molecular biology

#### Constructions of single and double mutants

Full length hERG channel was subcloned into the pSP64 vector (pSP64-hERG1a). Single and double mutants were constructed by using In-Fusion<sup>®</sup> HD Cloning Kit (TaKaRa). Two PCR primers including mutations were designed to elongate DNA fragments to upstream or downstream directions from the regions into which each mutation is introduced. PCR was performed using the designed forward primer with the reverse primer from BamHI restriction site region or the designed reverse primer with the forward primer from BstEII restriction site, and each template (pSP64-hERG1a or each single mutant). The obtained PCR fragments were purified and In-Fusion reaction was performed with vector side fragment of pSP64-hERG1a which was digested by BstEII and BamHI. After introduced into *E. coli* (TG1, Genotype; *supE*, *hsdΔ5*, *thi*,  $\Delta(lac-proAB)/F'$  [*traD36*, *proAB*<sup>+</sup>, *lac I*<sup>f</sup>, *lacZΔM15*] ),

each plasmid DNA was collected. The second mutations were introduced by subcloning the necessary region to intrinsic restriction sites in pSP64-hERG1a, using the restriction enzymes NcoI, BstEII, BglII, XhoI, SphI, BamHI and EcoRI (TOYOBO), and DNA Ligation Kit (TaKaRa). DNA sequences of all single and double mutants were confirmed using BigDye<sup>®</sup> Terminator v3.1 (Applied Biosystems) and the DNA sequencer (ABI PRISM 3130xl, Applied Biosystems). cRNA was transcribed from each linearized plasmid DNA using mMessage mMachine<sup>®</sup> SP6 Transcription Kit (Ambion).

### **Constructions of tandem constructs**

To make pSP64-hERG1a-hERG1a tandem construct (WT-(GGG)<sub>6</sub>-WT), a flexible GGS linker, (GGG)<sub>6</sub>, was introduced between the final amino acid residue (Ser1159) of the first hERG subunit and the initial amino acid residue (Met1) in the second hERG subunit using In-Fusion<sup>®</sup> HD Cloning Kit as described above. Each tandem construct including single or double mutations was subcloned as described above.

### **Electrophysiological experiments**

#### **Preparation of *Xenopus* oocytes**

All animal experiments in this study were approved by the Animal Care Committees of the National Institute for Physiological Sciences (Okazaki, Japan) and performed conforming to its guidelines. *Xenopus* oocytes were surgically collected from *Xenopus laevis* (Hamamatsu Animal Supply

Co.), after anesthesia in cold 0.15% tricaine water for 20 minutes. Collected oocytes were treated with collagenase (SIGMA) for 6-7 hours at room temperature to remove the follicle membranes. After selecting oocytes at stage V-VI, they were injected with 50 nl of 0.5  $\mu\text{g}/\mu\text{l}$  cRNA solution. The injected oocytes were incubated for 1 day (in case of tandem constructs, for 2 days) at 17°C in the frog ringer solution (88 mM NaCl, 1 mM KCl, 2.4 mM  $\text{NaHCO}_3$ , 0.3 mM  $\text{Ca}(\text{NO}_3)_2$ , 0.41 mM  $\text{CaCl}_2$  and 0.82 mM  $\text{MgSO}_4$ , pH 7.6, with 0.1% penicillin-streptomycin).

### **Two-Electrode Voltage Clamp experiments**

After 1-2 days from the injection, the macroscopic currents were recorded from injected oocytes under the two-electrode voltage clamp using an amplifier (OC-725C, Warner Instruments), a digidata (1322A, Axon), and the software for control and recording of voltage clamp (pCLAMP8.2, Axon). The glass microelectrodes were drawn from borosilicate glass capillaries (Harvard Apparatus), and filled with 3 M K-acetate and 10 mM KCl (pH 7.2). The resistance was 0.2-0.8 M $\Omega$ . All experiments were performed at room temperature (20-25°C). The bath solution was ND-96 (96 mM NaCl, 2 mM KCl, 1.8 mM  $\text{CaCl}_2$ , 1 mM  $\text{MgCl}_2$  and 5 mM HEPES, pH 7.4). Oocytes were voltage-clamped at -90 mV, and then two kinds of step pulse protocol were applied. The first protocol was to analyze voltage dependence; depolarizing step pulses from -80 to 60 mV for 2 s in 10 mV increments, followed by a step pulse to -60 mV for 2 s, every 8 s. The second protocol was to analyze the deactivation kinetics; a step to 40 mV for 1 s, followed by hyperpolarizing step pulses from -40 to -90 mV for 3 s in -10 mV

decrements, every 8 s. Data from the amplifier were digitized at 10 kHz and filtered at 1 kHz.

## **Data analyses**

### **Analyses of the deactivation kinetics**

The deactivation kinetics was analyzed by fitting the deactivation traces of the outward tail current to a double exponential function at each repolarizing voltage steps from -40 to -90 mV after depolarizing step at 40 mV, as follows.

$$f(t)=A_1e^{-t/\tau_1}+A_2e^{-t/\tau_2}+C$$

t value is time, and  $\tau_1$  and  $\tau_2$  values represent slow and fast time constants of the deactivation.  $A_1$  and  $A_2$  are fractions of each component. C is a constant component.

### **Analyses of the G-V relationship**

The relative conductance to the maximal one ( $G/G_{\max}$ ) was determined from the peak of the outward tail current at -60 mV after the depolarizing step pulses. The  $G/G_{\max}$  was plotted as a function of membrane potential, and the curve was fitted to the Boltzmann function, as follows.

$$f(V)=1/(1+e^{[(V_{1/2}-V)/k]})+C$$

$V_{1/2}$  value is the membrane potential when the G-V relationship reaches half level, and k value is the slope factor.

## **Statistical Analysis**

All averaged data are presented as mean $\pm$ SEM. n value is the number of recordings. A statistical significance between more than two groups was done by one-way analysis of variance (ANOVA) followed by Tukey's test. Values of  $P < 0.05$  were considered as statistically significant.

## Results

### Homology modeling of C-linker and CNB domains in hERG channel

To obtain the structural view of C-terminal region in hERG channel, I performed a homology modeling of C-linker and cyclic nucleotide binding (CNB) domains of hERG channel based on the monomeric crystal structure of *Anopheles gambiae* ERG (agERG) channel. Phe860 in hERG channel, a residue corresponding to Tyr740 in zELK channel, located in the ligand binding pocket (Figure 3B). Furthermore, there are two putative electrostatic interaction pairs similar to those of HCN and CNG channel. One is between Arg696 in C-linker domain and Asp767 in CNB domain, and another is between Arg696 and Asp727 in C-linker domain (Figure 1). By comparing the structure of CNB domain of hERG with that of mHCN2 channel, it was shown that  $\alpha$ A- and  $\alpha$ B-helices of CNB domain are located outside (Figure 3).

### Phe860 might fill the ligand binding pocket and control the slow deactivation

The homology modeling suggests a possibility that the Phe860 plays an important role for the gating of hERG channel (Figure 3). Therefore, I investigated the effects of various mutations at Phe860. Phe860 was substituted with small alanine (A), hydrophilic tyrosine (Y) which has a similar form to phenylalanine, hydrophobic isoleucine (I) and valine (V), positively charged arginine (R) and negatively charged glutamate (E).

First, I analyzed the effect on the slow deactivation, one of the most characteristic features of

hERG channel (Figure 4). The two time constants of deactivation ( $\tau_{\text{slow}}$ ,  $\tau_{\text{fast}}$ ) for F860I and F860V were not different from those of wild type (WT). The time constants for F860Y were slightly smaller than those of WT. In contrast, F860A, F860R and F860E showed accelerated deactivation (Table 1). Next, I analyzed the G-V relationship of each mutant channel because that of HCN channel shifts upon binding of the ligand. In contrast to the HCN channel, G-V relationship of each mutant was not different from that of WT (Figure 5). These results suggest that the presence of bulky amino acid residue Phe860, in the ligand binding pocket decelerates the deactivation, but does not give influence to the voltage dependence.

#### **A functional interaction between Arg696 and Asp767 in hERG1a channel**

There are the two possible electrostatic interacting pairs predicted from the homology modeling of hERG channel. First, I focused on the electrostatic interaction between Arg696 in C-linker domain and Asp767 in CNB domain (Figure 1). If Arg696 and Asp767 interact electrostatically to control the gating of hERG channel, it is thought that similar changes would be observed by single mutations of each amino acid residue disrupting the interaction. Furthermore, the charge reversions of both residues are expected to rescue the mutational effect of each single mutation. here, I substituted Arg696 and Asp767 with Glu and Lys which have opposite charges, respectively. A single point mutant R696E showed a slightly slower deactivation than WT, but G-V relationship was not changed (Figures 6, 7 and Table 1). Similar results were observed in R696D (Figure 8B, 9B and Table 1). In contrast, in D767K,

the deactivation was accelerated, and the G-V relationship was shifted negatively (Figures 6, 7 and Table 1). D767R also accelerated the deactivation, but G-V relationship was shifted positively (Figure 8B, 9B and Table 1). These results show that the Asp767 is important for channel gating, but Arg696 is not, and suggest that Arg696 and Asp767 do not interact directly.

However, the deactivation for a double mutant R696E&D767K became far slower than those of WT and each single mutant (Figure 6 and Table 1). If Arg696 and Asp767 were independent, the kinetics of R696E&D767K would be simply the sum of mutation effects of each single mutant. Thus, the result suggested that Arg696 and Asp767 are not independent. In the deactivation, similar results were observed in other charge reversal double mutants R696E&D767R, R696D&D767K and R696D&D767R (Figure 8 and Table 1). These results show that even though Arg696 and Asp767 do not interact directly with each other, they have a mutually dependent functional coupling, which controls the slow deactivation.

### **There is no clear interaction between Arg696 and Asp727**

Next, I analyzed the possible interaction between Arg696 and Asp727 in C-linker domain (Figure 1). As in the case of Arg696 and Asp767, I investigated the effects of substitution of Arg696 and Asp727 with Glu and Lys, respectively. In D727K mutant, the deactivation became faster than WT, and the G-V relationship shifted slightly to negative direction (Figures 10, 11 and Table 1). This phenotype is different from that of R696E. Similar results were observed in D727R (Figures 12, 13 and Table 1).

Therefore, as in the case of Arg696 and Asp767, it was suggested that Arg696 and Asp727 do not interact directly.

I also analyzed the phenotype of a double mutant R696E&D727K to examine the functional coupling between them. The deactivation time constants of a charge reversal double mutant, R696E&D727K, were similar to those of D727K (Figure 10 and Table 1). In addition, other double mutants, R696E&D727R, R696D&D727K and R696D&D727R, also showed similar results to each single mutant (Figure 12 and Table 1). Similar tendencies were also observed in G-V relationships (Figures 11, 13 and Table 1). These results suggest that there is no clear functional link between Arg696 and Asp727. This is in clear contrast with the case of mHCN2 channel.

### **Screening of the interaction partner with Asp727**

As it was shown that Arg696 is not an interaction partner with Asp727, I assumed that Asp727 electrostatically interacts with other amino acid residue(s). The candidate residue would have a positive charge, and its charge reversal mutant would show a similar phenotype to D727K. In addition, it was thought that the candidate is located close to Asp727. To search the candidate amino acid residues, I substituted all positively charged ones in C-liner and CNB domains with glutamate (only Arg791 to aspartate). Among these mutants, K748E, R752E, K759E, R784E, K801E, R814E, K817E, R835E and R863E showed significantly accelerated deactivation (Figure 14A), and Arg752 is located especially close to Asp727 in the homology model of hERG channel (Figure 14B). Then, I assumed

that Arg752 is the candidate of the interaction partner with Asp727.

### **A novel identification of an interaction between Asp727 and Arg752 in hERG channel**

If there is an interaction between Asp727 and Arg752, it is thought that the time constant of deactivation is recovered to the same level of WT in a charge reversal double mutant, D727K&R752E. Therefore, I analyzed the properties of D727K&R752E. As expected, the deactivation time constant of D727K&R752E was similar to that of WT (Figure 15 and Table 1). This result suggests that there is an electrical interaction between Asp727 and Arg752, which controls the slow deactivation. Another double mutant D727R&R752E also showed slow deactivation, similar to WT and D727K&R752E (Figure 16 and Table 1). D727K&R752D and D727R&R752D also showed a recovery of the slow deactivation from those of single mutants, but the extent of recovery was not very remarkable (Figure 17 and Table 1). In addition, D727K&R752E and D727R&R752E shifted the G-V relationships more negatively than the sum of each single mutant (Figures 16, 18 and Table 1). Also in this case, double mutants including R752D showed smaller effects than those including R752E (Figures 16, 18 and Table 1). These results suggest that the charge reversal double mutation including R752E is optimal for the restoration of interaction. Taken together, the results demonstrated that the electrostatic interaction between Asp727 and Arg752 are important for the slow deactivation.

### **Tandem construct experiments showed that both interactions are intra-subunit**

Based on the crystal structure of HCN channel, Lys472 and Asp542 are on the same subunit, whereas Glu502 is on the neighboring subunit. Therefore, the interaction between Lys472 and Asp542 in HCN channel is intra-subunit, and that of Lys472 and Glu502 is an inter-subunit one. By analogy, the interaction between Arg696 and Asp767 in hERG channel is expected to be intra-subunit one, and the newly identified Asp727 and Arg752 interaction is also intra-subunit. However, as the homology structure model of hERG channel is based on the monomeric crystal structure of agERG, there remain uncertainties about intra- or inter-subunit aspects. To determine if the interaction is intra- or inter-subunit, I made tandem constructs in which two subunits are connected by a flexible GGS linker (WT---WT) (Figure 19). For the analysis of the interaction between Arg696 and Asp767, I made three tandem constructs, WT---WT, R696E---D767K and R696E&D767K---WT (Figure 19). (Case 1) If the interaction between Arg696 and Asp767 is inter-subunit, tandem construct R696E---D767K has two intact and two charge reversal, in sum four, electrostatic interactions in the tetramer. In the case of R696E&D767K---WT, there would be no electrostatic interaction. Therefore, it is expected that R696E---D767K shows a normal slow deactivation like a double mutant R696E&D767K, and R696E&D767K---WT shows accelerated deactivation like D767K single mutant (Figure 19). (Case 2) However, if the interaction is within the intra-subunit, there will be no interaction in R696E---D767K, and four interactions will be maintained in R696E&D767K---WT, which has two intact and two charge reversal interactions. In this case, it is expected that R696E---D767K shows an accelerated deactivation, and R696E&D767K---WT shows a normal slow deactivation (Figure 19).

The results showed that the deactivation of R696E---D767K was faster, but that of R696E&D767K---WT was slower than that of WT---WT (Figure 20 and Table 1). These results demonstrate that the functional interaction between Arg696 and Asp767 is intra-subunit interaction. But, the deceleration effects in R696E&D767K---WT was smaller than the case of double mutant R696E&D767K (Figure 6). The difference might be due to the difference of the strength between WT and charge reversal interaction. Then, I made a tandem construct R696E&D767K---R696E&D767K having four charge reversal interactions. In this tandem construct, the deactivation speed became much slower than R696E&D767K---WT (Figure 20 and Table 1). These results additionally suggest that the time constant of deactivation changed depending on the number of charge reversal interactions.

Next, I performed similar analyses of the newly identified interaction pair, Arg696 and Asp767. D727K---R752E showed an accelerated deactivation, but D727K&R752E---WT showed a normal slow deactivation, similar to WT---WT (Figure 21 and Table 1). These results suggest that the interaction between Asp727 and Arg752 also is intra-subunit. In case of this interaction, D727K&R752E---D727K &R752E which have four charge reversal interactions showed similar results as D727K&R752E---WT (Figure 21 and Table 1).

## **Discussion**

In this study, I performed the homology modeling of the structure of C-linker and CNB domains of hERG channel based on the crystal structure of agERG channel. Based on this result, first, I analyzed the role of Phe860 in CNB domain in the gating of hERG channel. Second, I analyzed similarities and differences of the two electrostatic interactions between C-linker and CNG domains of hERG channel to those of HCN and CNG channels.

### **Phe860 in CNB domain in hERG channel which mimics the binding of cyclic nucleotides**

I performed the homology modeling of the structure of C-linker and the CNB domains of hERG channel based on the monomeric crystal structure of agERG channel in the same KCNH subfamily. The modeled structure showed Phe860 protrudes into the ligand binding pocket as Tyr740 in zELK channel does (Figure 3B). It was suggested that the ligand binding pocket of CNB domain of hERG channel is filled by Phe860, maintaining a similar structure to HCN channel in a cAMP bound state. I thus mutated the Phe860 to various amino acid residues to examine whether the disruption of the space filling affects the gating of the hERG channel or not.

The voltage dependence of HCN channel shifts to positive membrane potential upon cAMP binding to the ligand binding pocket, enhancing the channel activity (Craven & Zagotta, 2006). In zELK channel, the Y740A mutant and the truncated mutant from Tyr740 to Leu742 showed a positive shift of G-V relationship (Brelidze *et al.*, 2012). From these reports, I speculated that a voltage dependence

would be altered in hERG channel by substituting Phe860 to alanine, tyrosine, isoleucine, arginine, valine, or glutamate. Unexpectedly, all mutants did not show clear changes in the G-V relationship (Figure 5), suggesting that Phe860 of hERG channel did not participate in the control of voltage dependence unlike HCN and zELK channels. In contrast, mutations of Phe860 affected the slow deactivation to various extents (Figure 4).

The result of the homology modeling suggested that the ligand binding pocket of hERG channel is hydrophobic, so the side chain of a hydrophobic amino acid can bind easily. The substitution of Phe860 to hydrophobic isoleucine and valine did not clearly change the deactivation kinetics, and it was thought that the binding of a hydrophobic amino acid side chain to the ligand binding pocket maintained the structure of CNB domain of hERG channel to control the slow deactivation normally. When mutated to alanine, a small hydrophobic amino acid, the deactivation speed was accelerated. A substitution to hydrophilic but bulky tyrosine was also able to maintain the slow deactivation. A substitution to electrically charged arginine and glutamate accelerated the deactivation. Taken together, it was suggested that the hydrophobic interaction between amino acid residue at 860 and the ligand binding pocket in hERG channel underlies the structural stability of CNB domain and the characteristic slow deactivation.

In hERG channel, if Phe860 functions like a constitutively present ligand, it is thought that the structure of CNB domain observed from the homology modeling is in a ligand bound state. By comparing CNB domain of hERG channel with that of mHCN2 channel, it was shown that  $\alpha$ A- and

$\alpha$ B-helices of CNB domain are slightly translocated to outside (Figure 3B). A similar translocation was also observed in zELK, agERG and mEAG channels. In mHCN2 channel, it was shown that although cAMP bound into ligand binding pocket of CNB domain, the crystal structure was in close state (Craven & Zagotta, 2004). Therefore, it is thought the possibility that the state of CNB domain which is translocated  $\alpha$ A- and  $\alpha$ B-helices to outside is open state. In hERG channel, the acceleration of the deactivation observed in F860A, F860R and F860E mutant might be caused by a lack of outward translocation of  $\alpha$ A- and  $\alpha$ B-helices to outward.

**A functional, not direct, interaction between Arg696 in C-linker domain and Asp767 in CNB domain in hERG channel which controls the slow deactivation**

HCN channel has an intra-subunit interaction between Lys472 in C-linker domain and Asp542 in CNB domain, and an inter-subunit interaction between Lys472 and Glu502 in C-linker domain (Figure 1B). WT HCN channel is well known to show a positive shift of voltage dependence by the binding of cAMP. However, in K472E mutant, voltage dependence was shifted positively in the absence of cAMP, and no further change was observed when cAMP was applied. In K472E&D542K double mutant HCN channels, the WT phenotype was rescued (Craven & Zagotta, 2004). These results suggest that the electrostatic interaction between Lys472 and Asp542, which was impaired by K472E, was rescued by switching the position of the positively and negatively charged amino acid residues. Similar interactions are known also in CNG channel. CNG channel does not show voltage dependence, but opens upon

binding of cGMP, not cAMP. However, when the salt bridge was lost by a similar mutation as in HCN channel, this mutant was able to open by both cGMP and cAMP. Furthermore, a double mutant CNG channel, in which the positions of the positively and negatively charged residues were switched, showed similar properties to WT (Craven & Zagotta, 2004; Craven *et al.*, 2008). These results suggest that the salt bridge similar to that in HCN channel exist in CNG channel. In both channels, these electrostatic interactions are involved in the regulation mechanisms by cyclic-nucleotides. Both HCN and CNG channels have a tendency to become "easy to open" when the interactions are lost, suggesting that the interactions stabilize the close state of each channel, and that the binding cyclic-nucleotide into CNB domain might destroy the interactions, leading to opening of the channel gate.

The result of the homology modeling in this study suggested that C-linker and CNB domain of hERG channel also have similar interactions observed in HCN and CNG channels. In the present study, it was shown that CNB domain of hERG channel is in a state similar to the ligand bound state, as Phe860 constitutively fills the ligand binding pocket. Therefore, if the salt bridges of HCN and CNG channels are open upon ligand binding, it is speculated that the electrostatic interaction in hERG channel could be always open.

To confirm this speculation, I made hERG channel mutants which have reversed electrostatic charges, and analyzed the channel properties such as the deactivation kinetics and the G-V relationships (Figures 6-13). In hERG channel, the interactions shown by the homology modeling are between Arg696 in C-linker domain and Asp767 in CNB domain, and between Arg696 and Asp727 in C-linker

domain. First, when the electrostatic charge was reversed in Arg696, R696E and R696D did not show clear changes of the voltage dependence and the deactivation kinetics, in comparison with WT hERG channel. In contrast, when the electrostatic charges were reversed in Asp767 and Asp727, each single mutant showed different phenotypes from WT, such as accelerated deactivation. The difference of these mutation effects suggest that there are no direct electrostatic interactions between Arg696 and Asp767, and also Arg696 and Asp727 in hERG channel. This is in remarkable contrast with HCN and CNG channels. However, in Arg696 and Asp767 pair, not in Arg696 and Asp727 pair, the presence of "functional interaction" was suggested, because double charge reversal mutations restored the phenotype of slow deactivation (Figures 6, 8). The detail of this indirect, functional interaction remains to be studied, but it could be a tertiary interaction which involves another region. Furthermore, the result of the experiment using tandem constructs suggested that this functional interaction is intra-subunit interaction.

#### **A novel direct interaction between Asp727 and Arg752 in hERG channel which controls the slow deactivation**

The present results showed that there is no clear interaction between Asp727 and Arg696, which was expected by the homology modeling, but newly identified an electrostatic interaction between Asp727 and Arg752 in CNB domain (Figure 14). Both single reversal charge mutations at Asp727 and Arg752 of hERG channel significantly accelerated the deactivation (Figures 15, 17). If this acceleration

of the deactivation was caused by the loss the interaction, it was thought that the slow deactivation would be recovered by restoring the interaction. As expected, the slow deactivation was recovered by double mutants which have reversed electrostatic charges at both of Asp727 and Arg752 (Figures 15, 17). Taken together, it was shown that Asp727 and Arg752 directly interacted electrostatically, and the interaction is critical for the slow deactivation. Furthermore, the result of the tandem constructs experiment suggested that this electrostatic interaction is intra-subunit interaction.

A negatively charged amino acid residue at an equivalent to position of Asp727 is well conserved in HCN and CNG channels as well as in KCNH subfamily members including hERG channel (Figure 2). In contrast, the positively charged amino acid residue at Arg752 position is conserved only in KCNH subfamily, but not in HCN (threonine) or CNG (valine) channels (Figure 2B), showing that this electrostatic interaction between Asp727 and Arg752 exists only in the KCNH subfamily which lacks sensitivity to cyclic nucleotide.

This study showed that  $\alpha$ A- and  $\alpha$ B-helix of CNG domain of hERG and zELK channels are translocated outward in comparison with those of HCN channel (Figure 3B). Arg752 in hERG channel, newly identified as a pair of direct electrostatic interaction with Asp727, is located in  $\alpha$ A-helix. It is suggested that the mutant hERG channel such as F860A accelerate the deactivation by impairing the translocation of Arg752 and thus the interaction between Asp727 and Arg752.

It was reported that a mutation of Arg752 to tryptophan accelerates the deactivation and it is a cause of the inherited long QT syndrome (Ficker *et al.*, 2000). The cause of this acceleration might be a

loss of the interaction between Asp727 and Arg752. In addition, a recent report showed that the R752W mutation causes a mis-folding between EAG and CNB domain (Li *et al.*, 2016), suggesting that Arg752 binds to other sites nonspecifically when Arg752 cannot interact with Asp727.

### **Other mechanisms of C-linker and CNB domains contributing to the slow deactivation**

In this study, it was shown that C-linker and CNB domains of hERG channel are important to maintain the slow deactivation. In hERG channel, however, it is known that other regions such as N-terminal region also contribute to the slow deactivation. It was reported recently that CNB domain interacts with EAG domain, and this interaction is important to maintain the slow deactivation (Gustina & Trudeau, 2011; Fernandez-Trillo *et al.*, 2011; Gustina & Trudeau, 2013; Ng *et al.*, 2014; Haitin *et al.*, 2013), suggesting a possibility that the controlling mechanisms observed in this study influence this interaction.

In HCN and plant *Shaker* channels, it was showed that the C-linker domain interacts with S4-S5 linker to control the gating upon binding of cAMP (Prole & Yellen, 2006; Kwan *et al.*, 2012; Nieves-Cordones & Gaillard, 2014). In hERG channel, it is also known that S4-S5 linker is important to maintain the slow deactivation (Sanguinetti & Xu, 1999; Van Slyke *et al.*, 2010; Ng *et al.*, 2012; Hull *et al.*, 2014), by interacting with the N-tail domain (de la Pena *et al.*, 2011; de la Pena *et al.*, 2013; de la Pena *et al.*, 2014). It was suggested that S4-S5 linker domain could interact with C-linker domain to control the slow deactivation.

Finally, taken together, I found that the C-linker and CNB domains of hERG channel contribute to the control of slow deactivation by different mechanisms from HCN and CNG channels. These results showed the mechanisms that they did not elucidate in the C-terminal intracellular regions of hERG channel so far. It is thought that these new discoveries contribute to the future study of the hERG channel and the elucidation of the mechanisms of diseases which are due to the malfunction of hERG channel.

## References

- Akimoto M, Zhang Z, Boulton S, Selvaratnam R, VanSchouwen B, Gloyd M, Accili EA, Lange OF & Melacini G. (2014). A mechanism for the auto-inhibition of hyperpolarization-activated cyclic nucleotide-gated (HCN) channel opening and its relief by cAMP. *Journal of Biological Chemistry* **289**, 22205-22220.
- Al-Owais M, Bracey K & Wray D. (2009). Role of intracellular domains in the function of the herg potassium channel. *European Biophysics Journal* : EBJ **38**, 569-576.
- Aydar E & Palmer C. (2001). Functional characterization of the C-terminus of the human ether-a-go-go-related gene K(+) channel (HERG). *Journal of Physiology* **534**, 1-14.
- Brelidze TI, Carlson AE, Sankaran B & Zagotta WN. (2012). Structure of the carboxy-terminal region of a KCNH channel. *Nature* **481**, 530-533.
- Brelidze TI, Carlson AE & Zagotta WN. (2009). Absence of direct cyclic nucleotide modulation of mEAG1 and hERG1 channels revealed with fluorescence and electrophysiological methods. *Journal of Biological Chemistry* **284**, 27989-27997.
- Brelidze TI, Gianulis EC, Dimaio F, Trudeau MC & Zagotta WN. (2013). Structure of the C-terminal region of an ERG channel and functional implications. *Proceedings of the National Academy of Sciences of the United States of America* **110**, 11648-11653.
- Chen J, Zou A, Splawski I, Keating MT & Sanguinetti MC. (1999). Long QT syndrome-associated mutations in the Per-Arnt-Sim (PAS) domain of HERG potassium channels accelerate channel deactivation. *Journal of Biological Chemistry* **274**, 10113-10118.
- Cheng YM & Claydon TW. (2012). Voltage-dependent gating of HERG potassium channels. *Frontiers in Pharmacology* **3**, 83.
- Craven KB, Olivier NB & Zagotta WN. (2008). C-terminal movement during gating in cyclic nucleotide-modulated channels. *Journal of Biological Chemistry* **283**, 14728-14738.
- Craven KB & Zagotta WN. (2004). Salt bridges and gating in the COOH-terminal region of HCN2 and CNGA1 channels. *Journal of General Physiology* **124**, 663-677.
- Craven KB & Zagotta WN. (2006). CNG and HCN channels: two peas, one pod. *Annual Review of Physiology* **68**, 375-401.

- Curran ME, Splawski I, Timothy KW, Vincent GM, Green ED & Keating MT. (1995). A molecular basis for cardiac arrhythmia: HERG mutations cause long QT syndrome. *Cell* **80**, 795-803.
- de la Pena P, Alonso-Ron C, Machin A, Fernandez-Trillo J, Carretero L, Dominguez P & Barros F. (2011). Demonstration of physical proximity between the N terminus and the S4-S5 linker of the human ether-a-go-go-related gene (hERG) potassium channel. *Journal of Biological Chemistry* **286**, 19065-19075.
- de la Pena P, Machin A, Fernandez-Trillo J, Dominguez P & Barros F. (2013). Mapping of interactions between the amino and carboxy termini and the channel core in hERG K<sup>+</sup> channels. *Biochemical Journal* **451**, 463-474.
- de la Pena P, Machin A, Fernandez-Trillo J, Dominguez P & Barros F. (2014). Interactions between the N-terminal tail and the gating machinery of hERG K channels both in closed and open/inactive states. *Pflügers Archiv : European Journal of Physiology* **467**, 1747-1756.
- Fernandez-Trillo J, Barros F, Machin A, Carretero L, Dominguez P & de la Pena P. (2011). Molecular determinants of interactions between the N-terminal domain and the transmembrane core that modulate hERG K<sup>+</sup> channel gating. *PloS One* **6**, e24674.
- Ficker E, Thomas D, Viswanathan PC, Dennis AT, Priori SG, Napolitano C, Memmi M, Wible BA, Kaufman ES, Iyengar S, Schwartz PJ, Rudy Y & Brown AM. (2000). Novel characteristics of a misprocessed mutant HERG channel linked to hereditary long QT syndrome. *American Journal of Physiology Heart and Circulatory Physiology* **279**, H1748-1756.
- Flynn GE, Black KD, Islas LD, Sankaran B & Zagotta WN. (2007). Structure and rearrangements in the carboxy-terminal region of SpIH channels. *Structure (London, England : 1993)* **15**, 671-682.
- Foo B, Williamson B, Young JC, Lukacs G & Shrier A. (2016). hERG quality control and the long QT syndrome. *Journal of Physiology* **594**, 2469-2481.
- Frings S, Brull N, Dzeja C, Angele A, Hagen V, Kaupp UB & Baumann A. (1998). Characterization of ether-a-go-go channels present in photoreceptors reveals similarity to IKx, a K<sup>+</sup> current in rod inner segments. *Journal of General Physiology* **111**, 583-599.
- Gianulis EC & Trudeau MC. (2011). Rescue of aberrant gating by a genetically encoded PAS (Per-Arnt-Sim) domain in several long QT syndrome mutant human ether-a-go-go-related gene potassium channels. *Journal of Biological Chemistry* **286**, 22160-22169.

- Gustina AS & Trudeau MC. (2009). A recombinant N-terminal domain fully restores deactivation gating in N-truncated and long QT syndrome mutant hERG potassium channels. *Proceedings of the National Academy of Sciences of the United States of America* **106**, 13082-13087.
- Gustina AS & Trudeau MC. (2011). hERG potassium channel gating is mediated by N- and C-terminal region interactions. *Journal of General Physiology* **137**, 315-325.
- Gustina AS & Trudeau MC. (2012). HERG potassium channel regulation by the N-terminal eag domain. *Cellular Signalling* **24**, 1592-1598.
- Gustina AS & Trudeau MC. (2013). The eag domain regulates hERG channel inactivation gating via a direct interaction. *Journal of General Physiology* **141**, 229-241.
- Haitin Y, Carlson AE & Zagotta WN. (2013). The structural mechanism of KCNH-channel regulation by the eag domain. *Nature* **501**, 444-448.
- Hua L & Gordon SE. (2005). Functional interactions between A' helices in the C-linker of open CNG channels. *Journal of General Physiology* **125**, 335-344.
- Hull CM, Sokolov S, Van Slyke AC & Claydon TW. (2014). Regional flexibility in the S4-S5 linker regulates hERG channel closed-state stabilization. *Pflügers Archiv : European Journal of Physiology* **466**, 1911-1919.
- January CT, Gong Q & Zhou Z. (2000). Long QT syndrome: cellular basis and arrhythmia mechanism in LQT2. *Journal of Cardiovascular Electrophysiology* **11**, 1413-1418.
- Johnson JP, Jr. & Zagotta WN. (2001). Rotational movement during cyclic nucleotide-gated channel opening. *Nature* **412**, 917-921.
- Kaupp UB & Seifert R. (2002). Cyclic nucleotide-gated ion channels. *Physiological Reviews* **82**, 769-824.
- Ke Y, Ng CA, Hunter MJ, Mann SA, Heide J, Hill AP & Vandenberg JI. (2013). Trafficking defects in PAS domain mutant Kv11.1 channels: roles of reduced domain stability and altered domain-domain interactions. *Biochemical Journal* **454**, 69-77.
- Kesters D, Brams M, Nys M, Wijckmans E, Spurny R, Voets T, Tytgat J, Kusch J & Ulens C. (2015). Structure of the SthK carboxy-terminal region reveals a gating mechanism for cyclic nucleotide-modulated ion channels. *PLoS One* **10**, e0116369.

- Kwan DC, Prole DL & Yellen G. (2012). Structural changes during HCN channel gating defined by high affinity metal bridges. *Journal of General Physiology* **140**, 279-291.
- Li Q, Ng HQ, Yoon HS & Kang C. (2014). Solution structure of the cyclic-nucleotide binding homology domain of a KCNH channel. *Journal of Structural Biology* **186**, 68-74.
- Li Y, Ng HQ, Li Q & Kang C. (2016). Structure of the Cyclic Nucleotide-Binding Homology Domain of the hERG Channel and Its Insight into Type 2 Long QT Syndrome. *Scientific Reports* **6**, 23712.
- Morais-Cabral JH & Robertson GA. (2015). The enigmatic cytoplasmic regions of KCNH channels. *Journal of Molecular Biology* **427**, 67-76.
- Morais Cabral JH, Lee A, Cohen SL, Chait BT, Li M & Mackinnon R. (1998). Crystal structure and functional analysis of the HERG potassium channel N terminus: a eukaryotic PAS domain. *Cell* **95**, 649-655.
- Muskett FW, Thouta S, Thomson SJ, Bowen A, Stansfeld PJ & Mitcheson JS. (2011). Mechanistic insight into human ether-a-go-go-related gene (hERG) K<sup>+</sup> channel deactivation gating from the solution structure of the EAG domain. *Journal of Biological Chemistry* **286**, 6184-6191.
- Ng CA, Hunter MJ, Perry MD, Mobli M, Ke Y, Kuchel PW, King GF, Stock D & Vandenberg JI. (2011). The N-terminal tail of hERG contains an amphipathic alpha-helix that regulates channel deactivation. *PloS One* **6**, e16191.
- Ng CA, Perry MD, Tan PS, Hill AP, Kuchel PW & Vandenberg JI. (2012). The S4-S5 linker acts as a signal integrator for HERG K<sup>+</sup> channel activation and deactivation gating. *PloS One* **7**, e31640.
- Ng CA, Phan K, Hill AP, Vandenberg JI & Perry MD. (2014). Multiple Interactions between Cytoplasmic Domains Regulate Slow Deactivation of Kv11.1 Channels. *Journal of Biological Chemistry* **289**, 25822-25832.
- Nieves-Cordones M & Gaillard I. (2014). Involvement of the S4-S5 linker and the C-linker domain regions to voltage-gating in plant Shaker channels: comparison with animal HCN and Kv channels. *Plant Signaling & Behavior* **9**, e972892.
- Perry MD, Ng CA, Mann SA, Sadrieh A, Imtiaz M, Hill AP & Vandenberg JI. (2015). Getting to the heart of hERG K(+) channel gating. *Journal of Physiology* **593**, 2575-2585.

- Piper DR, Hinz WA, Tallurri CK, Sanguinetti MC & Tristani-Firouzi M. (2005). Regional specificity of human ether-a'-go-go-related gene channel activation and inactivation gating. *Journal of Biological Chemistry* **280**, 7206-7217.
- Prole DL & Yellen G. (2006). Reversal of HCN channel voltage dependence via bridging of the S4-S5 linker and Post-S6. *Journal of General Physiology* **128**, 273-282.
- Roden DM. (2006). Long QT syndrome: reduced repolarization reserve and the genetic link. *Journal of Internal Medicine* **259**, 59-69.
- Sands Z, Grottesi A & Sansom MS. (2005). Voltage-gated ion channels. *Current Biology : CB* **15**, R44-47.
- Sanguinetti MC. (2010). HERG1 channelopathies. *Pflugers Archiv : European Journal of Physiology* **460**, 265-276.
- Sanguinetti MC, Jiang C, Curran ME & Keating MT. (1995). A mechanistic link between an inherited and an acquired cardiac arrhythmia: HERG encodes the IKr potassium channel. *Cell* **81**, 299-307.
- Sanguinetti MC & Tristani-Firouzi M. (2006). hERG potassium channels and cardiac arrhythmia. *Nature* **440**, 463-469.
- Sanguinetti MC & Xu QP. (1999). Mutations of the S4-S5 linker alter activation properties of HERG potassium channels expressed in *Xenopus* oocytes. *Journal of Physiology* **514**, 667-675.
- Schonherr R & Heinemann SH. (1996). Molecular determinants for activation and inactivation of HERG, a human inward rectifier potassium channel. *Journal of Physiology* **493**, 635-642.
- Schunke S, Stoldt M, Lecher J, Kaupp UB & Willbold D. (2011). Structural insights into conformational changes of a cyclic nucleotide-binding domain in solution from *Mesorhizobium loti* K1 channel. *Proceedings of the National Academy of Sciences of the United States of America* **108**, 6121-6126.
- Schunke S, Stoldt M, Novak K, Kaupp UB & Willbold D. (2009). Solution structure of the *Mesorhizobium loti* K1 channel cyclic nucleotide-binding domain in complex with cAMP. *EMBO Reports* **10**, 729-735.

- Shimizu W. (2008). Clinical impact of genetic studies in lethal inherited cardiac arrhythmias. *Circulation journal : Official Journal of the Japanese Circulation Society* **72**, 1926-1936.
- Smith PL & Yellen G. (2002). Fast and slow voltage sensor movements in HERG potassium channels. *Journal of General Physiology* **119**, 275-293.
- Spector PS, Curran ME, Zou A, Keating MT & Sanguinetti MC. (1996). Fast inactivation causes rectification of the IKr channel. *Journal of General Physiology* **107**, 611-619.
- Tan PS, Perry MD, Ng CA, Vandenberg JI & Hill AP. (2012). Voltage-sensing domain mode shift is coupled to the activation gate by the N-terminal tail of hERG channels. *Journal of General Physiology* **140**, 293-306.
- Thouta S, Sokolov S, Abe Y, Clark SJ, Cheng YM & Claydon TW. (2014). Proline scan of the HERG channel s6 helix reveals the location of the intracellular pore gate. *Biophysical Journal* **106**, 1057-1069.
- Tombola F, Pathak MM & Isacoff EY. (2006). How does voltage open an ion channel? *Annual Review of Cell and Developmental Biology* **22**, 23-52.
- Trudeau MC, Leung LM, Roti ER & Robertson GA. (2011). hERG1a N-terminal eag domain-containing polypeptides regulate homomeric hERG1b and heteromeric hERG1a/hERG1b channels: a possible mechanism for long QT syndrome. *Journal of General Physiology* **138**, 581-592.
- Trudeau MC, Warmke JW, Ganetzky B & Robertson GA. (1995). HERG, a human inward rectifier in the voltage-gated potassium channel family. *Science* **269**, 92-95.
- Van Slyke AC, Rezazadeh S, Snopkowski M, Shi P, Allard CR & Claydon TW. (2010). Mutations within the S4-S5 linker alter voltage sensor constraints in hERG K<sup>+</sup> channels. *Biophysical Journal* **99**, 2841-2852.
- Vandenberg JI, Perry MD, Perrin MJ, Mann SA, Ke Y & Hill AP. (2012). hERG K(+) channels: structure, function, and clinical significance. *Physiological Reviews* **92**, 1393-1478.
- Wahl-Schott C & Biel M. (2009). HCN channels: structure, cellular regulation and physiological function. *Cellular and Molecular Life Sciences : CMLS* **66**, 470-494.
- Wang J, Myers CD & Robertson GA. (2000). Dynamic control of deactivation gating by a soluble

amino-terminal domain in HERG K(+) channels. *Journal of General Physiology* **115**, 749-758.

Warmke JW & Ganetzky B. (1994). A family of potassium channel genes related to eag in *Drosophila* and mammals. *Proceedings of the National Academy of Sciences of the United States of America* **91**, 3438-3442.

Wynia-Smith SL, Gillian-Daniel AL, Satyshur KA & Robertson GA. (2008). hERG gating microdomains defined by S6 mutagenesis and molecular modeling. *Journal of General Physiology* **132**, 507-520.

Zagotta WN, Olivier NB, Black KD, Young EC, Olson R & Gouaux E. (2003). Structural basis for modulation and agonist specificity of HCN pacemaker channels. *Nature* **425**, 200-205.

Zhang M, Liu J & Tseng GN. (2004). Gating charges in the activation and inactivation processes of the HERG channel. *Journal of General Physiology* **124**, 703-718.

## Figure 1

### A schematic drawing of hERG channel and tetrameric structure of mHCN channel

**A)** A schematic drawing of the structure of human ERG (hERG) channel monomer. There are six transmembrane segments (S1-S6). There are N-tail and Per-Arnt-Sim (PAS) domains in the N-terminal intracellular region. The C-linker domain (666-747 amino acid residues) and the cyclic nucleotide binding (CNB) domain (748-872 amino acid residues) are colored in yellow and green, respectively. **B)** The tetrameric structure of the C-linker domain and the CNB domain of mouse HCN2 (mHCN2) channel (PDB: 1Q43). Lys472 in C-linker domain is colored in blue, and Asp542 in CNB domain of the same subunit is colored in red. They correspond to Arg696 and Asp767 in hERG1a channel, respectively. Glu502 in C-linker domain of the neighboring subunit is colored in red. It corresponds to Asp727 in hERG channel.

## Figure 2

### Sequence alignments of C-linker and CNB domain of mHCN2, bCNGA1, zELK, agERG and hERG channels

**A)** The amino acid sequences of the C-linker domains of mHCN2, bovine CNGA1 (bCNGA1), zebrafish ELK (zELK), *Anopheles gambiae* ERG (agERG) and hERG channels. Yellow solid squares on sequences show  $\alpha$ -helix. Amino acid residues framed by a blue square show Lys472 in mHCN2, Arg431 in bCNGA1, Arg575 in zELK, Arg563 in agERG and Arg696 in hERG channel. Amino acid residues

framed by a red square show Glu502 in mHCN2, Glu462 in bCNGA1, Asp606 in zELK, Asp594 in agERG and Asp727 in hERG channel. **B)** The amino acid sequences of the CNB domains of mHCN2, bCNGA1, zELK, agERG and hERG channels. Green solid squares and green solid arrows show  $\alpha$ -helix and  $\beta$ -sheet, respectively. Amino acid residues framed by a red square show Asp542 in mHCN2, Asp502 in bCNGA1, Glu645 in zELK, Asp634 in agERG and Asp767 in hERG channel. Amino acid residues framed by a purple square show Tyr740 in zELK, Tyr727 in agERG and Phe860 in hERG channel. A blue frame in a broken line highlights Arg752 in hERG channel.

### **Figure 3**

**The tree diagram of HCN, CNG and KCNH families and structures of CNB domain of mHCN2, zELK, agERG and hERG channels**

**A)** The tree diagram of HCN, CNG and KCNH families. zELK channel belongs to KCNH3, 4 or 8, and agERG belongs to KCNH2, 6 or 7. **B)** The crystal structures of the CNB domains of mHCN2 (PDB: 1Q43), zELK (PDB: 3UKN) and agERG (PDB: 4L11) channels, and the structure model of the CNB domain of hERG channel obtained by homology modeling based on the monomeric structure of agERG channel using SWISS-MODEL server. cAMP in mHCN2, Tyr740 in zELK, Tyr727 in agERG and Phe860 in hERG channel are highlighted in purple.  $\alpha$ A,  $\alpha$ B and  $\alpha$ C are  $\alpha$ -helices in Figure 2B.

### **Figure 4**

### The deactivation kinetics of a series of Phe860 mutants

**A)** The deactivating tail current traces of wild type (WT, ●), F860A (■), F860Y (▲), F860I (▼), F860R (◆), F860V (▶) and F860E (◀) hERG channel, recorded from *Xenopus* oocytes under two electrode voltage clamp. The used pulse protocol is indicated in the upper right panel, and each current at -60 mV is colored in red. **B)** The time constants ( $\tau$ ) of deactivation for WT and mutant hERG channels in panel A. Each deactivating tail current was fitted to a double exponential function to determine the slow ( $\tau_{\text{slow}}$ ) and fast ( $\tau_{\text{fast}}$ ) time constants and the values (mean $\pm$ SEM (n=5)) were plotted as a function of membrane potential. The errors are less than the symbol size where the error bars are not visible.

### Figure 5

#### The G-V relationships of a series of Phe860 mutants

**A)** The current traces of WT (●), F860A (■), F860Y (▲), F860I (▼), F860R (◆), F860V (▶) and F860E (◀) hERG channel recorded from *Xenopus* oocytes under two electrode voltage clamp. The used pulse protocol is indicated in the upper right panel, and each current at 0 mV is colored in red. **B)** G-V relationships for WT and mutant hERG channels in panel A. The peaks of tail currents at -60 mV were normalized to the maximum tail current in each cell, and plotted as a function of membrane potential. The data were fitted to a Boltzmann function to determine the  $V_{1/2}$  values. The values are plotted as the mean $\pm$ SEM (n=5), and the errors are less than the symbol size where the error bars are not

visible.  $V_{1/2}$  values are indicated on the right side of G-V relationships as the mean $\pm$ SEM (n=5).

## Figure 6

### The deactivation kinetics of R696E, D767K and R696E&D767K

**A)** The deactivating tail current traces of WT (●), R696E (■), D767K (▲) and R696E&D767K (◇) hERG channel recorded from *Xenopus* oocytes under two electrode voltage clamp. The used pulse protocol is indicated in the lower left panel, and each current at -70 mV is colored in red. **B)** The time constants ( $\tau$ ) of deactivation for WT and mutant hERG channels in panel A. Each deactivating tail current was fitted to a double exponential function to determine the  $\tau_{\text{slow}}$  and  $\tau_{\text{fast}}$ , and the values (mean $\pm$ SEM (n=5)) were plotted as a function of membrane potential. The errors are less than the symbol size where the error bars are not visible.

## Figure 7

### The G-V relationships of R696E, D767K and R696E&D767K

**A)** The current traces of WT (●), R696E (■), D767K (▲) and R696E&D767K (◇) hERG channel recorded from *Xenopus* oocytes under two electrode voltage clamp. The used pulse protocol is indicated in the lower left panel, and each current at 0 mV is colored in red. **B)** G-V relationships for WT and mutant hERG channels in panel A. The peaks of tail currents at -60 mV were normalized to the maximum tail current in each cell, and plotted as a function of membrane potential. The data were fitted

to a Boltzmann function to determine the  $V_{1/2}$  values. The values are plotted as the mean $\pm$ SEM (n=5), and the errors are less than the symbol size where the error bars are not visible.  $V_{1/2}$  values are indicated on the right side of G-V relationships as the mean $\pm$ SEM (n=5).

### Figure 8

**The deactivation kinetics of R696E&D767K, R696E&D767R, R696D&D767K and R696D&D767R**

**A)** The deactivating tail current traces of WT (●), R696E&D767K (◇), R696E&D767R (◇), R696D&D767K (◇) and R696D&D767R (◇) hERG channel recorded from *Xenopus* oocytes under two electrode voltage clamp. The used pulse protocol is indicated in the upper right panel, and each current at -70 mV is colored in red. **B)** The time constants ( $\tau$ ) of deactivation for WT and the double mutant hERG channels in panel A, for R696E (■) and D767K (▲) from figure 06, and for R696D (■) and D767R (▲) traces of which were not shown. Each deactivating tail current was fitted to a double exponential function to determine the  $\tau_{\text{slow}}$  and  $\tau_{\text{fast}}$ , and the values (mean $\pm$ SEM (n=5)) were plotted as a function of membrane potential. The errors are less than the symbol size where the error bars are not visible.

### Figure 9

**The G-V relationships of R696E&D767K, R696E&D767R, R696D&D767K and R696D&D767R**

**A)** The current traces of WT (●), R696E&D767K (◇), R696E&D767R (◇), R696D&D767K (◇) and R696D&D767R (◇) hERG channel recorded from *Xenopus* oocytes under two electrode voltage clamp. The used pulse protocol is indicated in the upper right panel, and each current at 0 mV is colored in red. **B)** G-V relationships for WT and the double mutant hERG channels in panel A, for R696E (■) and D767K (▲) from figure 07, and for R696D (■) and D767R (▲) traces of which were not shown. The peaks of tail currents at -60 mV were normalized to the maximum tail current in each cell, and plotted as a function of membrane potential. The data were fitted to a Boltzmann function to determine the  $V_{1/2}$  value. The values are plotted as the mean±SEM (n=5), and the errors are less than the symbol size where the error bars are not visible.  $V_{1/2}$  values are indicated on the right side of G-V relationships as the mean±SEM (n=5).

## Figure 10

### The deactivation kinetics of R696E, D727K and R696E&D727K

**A)** The deactivating tail current traces of WT (●), R696E (■), D727K (▼) and R696E&D727K (◇) hERG channel recorded from *Xenopus* oocytes under two electrode voltage clamp. The used pulse protocol is indicated in the lower left panel, and each current at -60 mV is colored in red. **B)** The time constants ( $\tau$ ) of deactivation for WT and mutant hERG channels in panel A. Each deactivating tail current was fitted to a double exponential function to determine the  $\tau_{\text{slow}}$  and  $\tau_{\text{fast}}$ , and the values (mean±SEM (n=5)) were plotted as a function of membrane potential. The errors are less than the

symbol size where the error bars are not visible.

## Figure 11

### The G-V relationships of R696E, D727K and R696E&D727K

A) The current traces of WT (●), R696E (■), D727K (▼) and R696E&D727K (◇) hERG channel recorded from *Xenopus* oocytes under two electrode voltage clamp. The used pulse protocol indicated in the lower left panel, and each current at 0 mV is colored in red. B) G-V relationships for WT and mutant hERG channels in panel A. The peaks of tail currents at -60 mV were normalized to the maximum tail current in each cell, and plotted as a function of membrane potential. The data were fitted to a Boltzmann function to determine the  $V_{1/2}$  values. The values are plotted as the mean±SEM (n=5), and the errors are less than the symbol size where the error bars are not visible.  $V_{1/2}$  values are indicated on the right side of G-V relationships as the mean±SEM (n=5).

## Figure 12

### The deactivation kinetics of R696E&D727K, R696E&D727R, R696D&D727K and R696D&D727R

A) The deactivating tail current traces of WT (●), R696E&D727K (◇), R696E&D727R (◇), R696D&D727K (◇) and R696D&D727R (◇) hERG channel recorded from *Xenopus* oocytes under two electrode voltage clamp. The used pulse protocol is indicated in the upper right panel, and each

current at -70 mV is colored in red. **B)** The time constants ( $\tau$ ) of deactivation for WT and the double mutant hERG channels in panel A, for R696E (■) and D727K (▼) from figure 10, and for R696D (■) and D727R (▼) traces of which were not shown. Each deactivating tail current was fitted to a double exponential function to determine the  $\tau_{\text{slow}}$  and  $\tau_{\text{fast}}$ , and the values (mean $\pm$ SEM (n=5)) were plotted as a function of membrane potential. The errors are less than the symbol size where the error bars are not visible.

### Figure 13

#### The G-V relationships of R696E&D727K, R696E&D727R, R696D&D727K and R696D&D727R

**A)** The current traces of WT (●), R696E&D727K (◇), R696E&D727R (◇), R696D&D727K (◇) and R696D&D727R (◇) hERG channel recorded from *Xenopus* oocytes under two electrode voltage clamp. The used pulse protocol is indicated in the upper right panel, and each current at 0 mV is colored in red. **B)** G-V relationships for WT and the double mutant hERG channels in panel A, for R696E (■) and D727K (▼) from figure 11, and for R696D (■) and D727R (▼) traces of which were not shown. The peaks of tail currents at -60 mV were normalized to the maximum tail current in each cell, and plotted as a function of membrane potential. The data were fitted to a Boltzmann function to determine the  $V_{1/2}$  value. The values are plotted as the mean $\pm$ SEM (n=5), and the errors are less than the symbol size where the error bars are not visible.  $V_{1/2}$  values are indicated on the right side of G-V relationships as the mean $\pm$ SEM (n=5).

## Figure 14

### A screening for candidate amino acid residues interacting with Asp727

**A)** The time constants of deactivation at -70 mV for WT and charge reversal mutant hERG channel. In the mutants, each positively charged amino acid residue in C-linker domain and CNB domain was mutated to negatively charged Glu or Asp. Upper and lower panels show  $\tau_{\text{slow}}$  and  $\tau_{\text{fast}}$ , respectively. Bars represent the mean $\pm$ SEM (WT; n=64, each mutant; n=3-5). \* stands for the value of  $P < 0.05$  versus WT. **B)** A monomeric structure model of the C-linker domain and CNB domain of hERG channel obtained by homology modeling based on zELK channel. The C-linker and the CNB domains are respectively colored in yellow and green. Side chains of all Arg and Lys are shown. Asp727 is colored in red, and the mutants which showed significantly smaller slow and fast time constants compared with those of WT are colored in blue.

## Figure 15

### The deactivation kinetics of D727K, R752E and D727K&R752E

**A)** The deactivating tail current traces of WT (●), D727K (▼), R752E (■) and D727K&R752E (◇) hERG channel recorded from *Xenopus* oocytes under two electrode voltage clamp. The used pulse protocol is indicated in the lower left panel, and each current at -60 mV is colored in red. **B)** The time constants ( $\tau$ ) of deactivation for WT and mutant hERG channels in panel A. Each deactivating tail

current was fitted to a double exponential function to determine the  $\tau_{\text{slow}}$  and  $\tau_{\text{fast}}$ , and the values (mean $\pm$ SEM (n=5)) were plotted as a function of membrane potential. The errors are less than the symbol size where the error bars are not visible.

## Figure 16

### The G-V relationships of D727K, R752E and D727K&R752E

A) The current traces of WT (●), D727K (▼), R752E (■) and D727K&R752E (◇) hERG channel recorded from *Xenopus* oocytes under two electrode voltage clamp. The used pulse protocol is indicated in the lower left panel, and each current at 0 mV is colored in red. B) G-V relationships for WT and mutant hERG channels in panel A. The peaks of tail currents at -60 mV were normalized to the maximum tail current in each cell, and plotted as a function of membrane potential. The data were fitted to a Boltzmann function to determine the  $V_{1/2}$  values. The values are plotted as the mean $\pm$ SEM (n=5), and the errors are less than symbol size where the error bars are not visible.  $V_{1/2}$  values are indicated on the right side of G-V relationships as the mean $\pm$ SEM (n=5).

## Figure 17

### The deactivation kinetics of D727K&R752E, D727K&R752D, D727R&R752E and D727R&R752D

A) The deactivating tail current traces of WT (●), D727K&R752E (◇), D727K&R752D (◇),

D727R&R752E (◇) and D727R&R752D (◇) hERG channel recorded from *Xenopus* oocytes under two electrode voltage clamp. The used pulse protocol is indicated in the upper right panel, and each current at -70 mV is colored in red. **B)** The time constants ( $\tau$ ) of deactivation for WT and the double mutant hERG channels in panel A, for D727K (▼) and R752E (■) from figure 15, and for D727R (▼) and R752D (■) traces of which were not shown. Each deactivating tail current was fitted to a double exponential function to determine the  $\tau_{\text{slow}}$  and  $\tau_{\text{fast}}$ , and the values (mean $\pm$ SEM (n=5)) were plotted as a function of membrane potential. The errors are less than the symbol size where the error bars are not visible.

## Figure 18

### The G-V relationships of D727K&R752E, D727K&R752D, D727R&R752E and D727R&R752D

**A)** The current traces of WT (●), D727K&R752E (◇), D727K&R752D (◇), D727R&R752E (◇) and D727R&R752D (◇) hERG channel recorded from *Xenopus* oocytes under two electrode voltage clamp. The used pulse protocol is indicated in the upper right panel, and each current at 0 mV is colored in red. **B)** G-V relationships for WT and the double mutant hERG channels in panel A, for D727K (▼) and R752E (■) from figure 16, and for D727R (▼) and R752D (■) traces of which were not shown. The peaks of tail currents at -60 mV were normalized to the maximum tail current in each cell, and plotted as a function of membrane potential. The data were fitted to a Boltzmann function to determine the  $V_{1/2}$  value. The values are plotted as the mean $\pm$ SEM (n=5), and the errors are less than the

symbol size where the error bars are not visible.  $V_{1/2}$  values are indicated on the right side of G-V relationships as the mean $\pm$ SEM (n=5).

## Figure 19

### A Schematic drawing of the tandem repeat construct and expected numbers of electrostatic pairs in mutants

**A)** A schematic drawing of the tandem construct of hERG1a channel. Two subunits of full length hERG1a channel were ligated by a flexible linker residues (GGS)<sub>6</sub>. The C-linker domain and the CNB domain are colored in yellow and green, respectively. **B)** A scheme explaining the numbers of electrostatic pairs in mutants in each case of “inter” or “intra” subunit interaction. If the interaction is inter-subunit, A---B tandem construct is expected to have four interactions, while A&B---WT has no interaction. In contrast, if the interaction is intra-subunit, A---B is expected to have no interaction, while A&B---WT has four interactions.

## Figure 20

### The deactivation kinetics of a series of tandem constructs in relation to the interaction between R696 and D767

**A)** The deactivating tail current traces of WT---WT (●), R696E---D767K (▲), R696E&D767K---WT (▼) and R696E&D767K---R696E&D767K (■) hERG channel, recorded from m

*Xenopus* oocytes under two electrode voltage clamp. The used pulse protocol is indicated in the upper right panel, and each current at -60 mV is colored in red. Schematic drawings show each tandem construct including mutations. **B)** The time constants ( $\tau$ ) of deactivation for the tandem construct hERG channels in panel A. Each deactivating tail current was fitted to a double exponential function to determine the  $\tau_{\text{slow}}$  and  $\tau_{\text{fast}}$ , and the values (mean $\pm$ SEM (n=5)) were plotted as a function of membrane potential. The errors are less than the symbol size where the error bars are not visible.

## Figure 21

### The deactivation kinetics of a series of tandem constructs in relation to the interaction between D727 and R752

**A)** The deactivating tail current traces of WT---WT (●), D727K---R752E (▲), D727K&R752E---WT (▼) and D727K&R752E---D727K&R752E (■) hERG channel recorded from *Xenopus* oocytes under two electrode voltage clamp. The used pulse protocol is indicated in the upper right panel, and each current at -60 mV is colored in red. Schematic drawings show each tandem construct including mutations. **B)** The time constants ( $\tau$ ) of deactivation for the tandem construct hERG channels in panel A. Each deactivating tail current was fitted to a double exponential function to determine the  $\tau_{\text{slow}}$  and  $\tau_{\text{fast}}$ , and the values (mean $\pm$ SEM (n=5)) were plotted as a function of membrane potential. The errors are less than the symbol size where the error bars are not visible.

## Figure 22

### **A schematic drawing of the electrostatic interaction of C-linker and CNB domain of hERG channel in comparison with mHCN2 channel**

**A)** A schematic drawing of human ERG (hERG) channel monomer. The N-terminal region is omitted. C-linker and CNB domains are colored in yellow and green, respectively. **B)** The tetrameric structure of the C-linker and the CNB domains of mHCN2 channel (PDB: 1Q43). Lys472 in C-linker domain is colored in blue, and Asp542 in CNB domain of the same subunit is colored in red. Glu502 in C-linker domain of the neighboring subunit is colored in red. cAMP in mHCN2 channel is highlighted in red. Red ovals indicate the direct electrostatic interactions. **C)** The structure of the C-linker and the CNB domain of hERG channel obtained by a homology modeling based on the structure of agERG channel monomer (PDB: 4L11). As information as to multimerization is missing in agERG, tetramerization view is based on those of mHCN2 channel. Arg696 in C-linker domain is colored in blue, and Asp767 in CNB domain of the same subunit is colored in red. Asp727 in C-linker domain of the neighboring subunit is colored in red, and Arg752 in CNB domain is colored in blue. Phe860 is highlighted in red. A dotted red oval indicates the indirect functional interaction, and blue one indicates the newly identified direct electrostatic interaction.

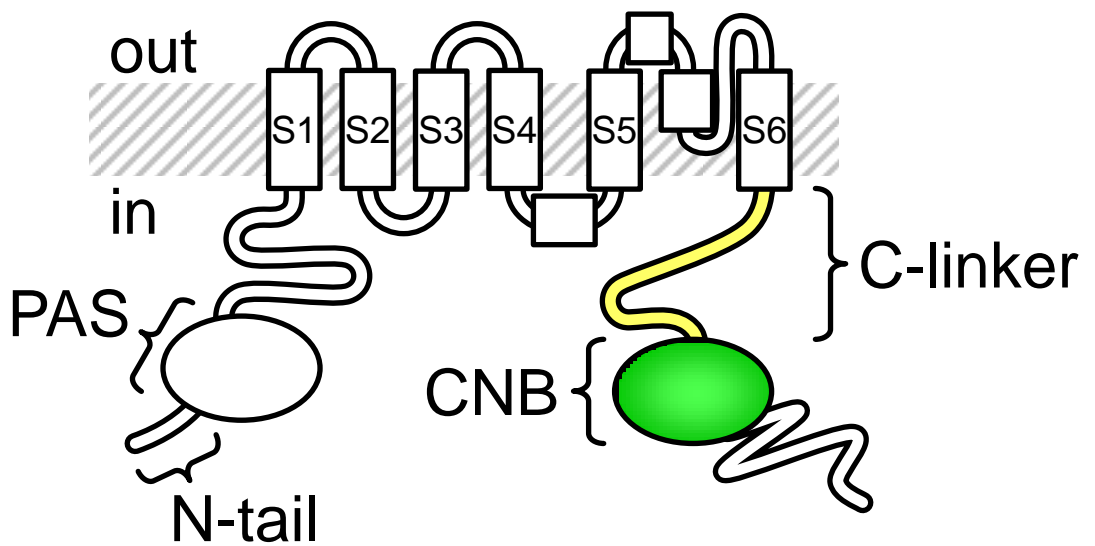
**Table 1**

Summary of the parameter of deactivation and G-V relationship of WT and mutants analysed in this study

	$\tau_{\text{slow}}$ at -70 mV (ms)	$\tau_{\text{fast}}$ at -70 mV (ms)	$V_{1/2}$ (mV)	n
WT	822.0 ± 22.4	188.8 ± 6.6	-20.2 ± 0.5	5
F860A	372.0 ± 10.8	103.2 ± 3.1	-24.4 ± 0.4	5
F860Y	573.6 ± 13.3	142.7 ± 1.6	-21.2 ± 0.3	5
F860I	773.9 ± 28.9	177.9 ± 8.7	-22.4 ± 0.5	5
F860R	227.8 ± 6.3	59.7 ± 1.2	-21.3 ± 0.6	5
F860V	750.7 ± 23.3	172.6 ± 6.6	-22.3 ± 0.9	5
F860E	291.8 ± 49.4	39.3 ± 0.8	-21.7 ± 1.3	5
WT	822.6 ± 51.7	204.4 ± 15.9	-18.3 ± 0.5	5
R696E	1050.4 ± 71.9	219.6 ± 10.3	-16.8 ± 0.4	5
R696D	1074.1 ± 27.7	234.5 ± 6.5	-16.2 ± 0.3	5
D767K	324.1 ± 5.4	97.3 ± 2.5	-26.0 ± 0.6	5
D767R	509.7 ± 8.1	129.2 ± 4.1	-10.2 ± 0.3	5
R696E&D767K	2638.3 ± 379.7	521.2 ± 94.8	-32.2 ± 1.0	5
R696E&D767R	1270.4 ± 27.5	277.6 ± 9.8	-11.7 ± 0.5	5
R696D&D767K	2227.7 ± 184.3	424.5 ± 56.5	-29.3 ± 0.5	5
R696D&D767R	1735.7 ± 45.2	319.0 ± 4.9	-19.5 ± 0.2	5
WT	849.3 ± 42.2	209.7 ± 9.8	-18.1 ± 0.6	5
R696E	1264.1 ± 13.9	270.9 ± 1.5	-17.0 ± 0.3	5
R696D	1136.1 ± 52.6	239.1 ± 10.7	-15.1 ± 0.2	5
D727K	406.2 ± 2.6	121.7 ± 2.6	-22.6 ± 0.4	5
D727R	645.1 ± 22.2	177.1 ± 6.5	-24.4 ± 0.6	5
R696E&D727K	471.4 ± 5.9	136.5 ± 3.4	-22.3 ± 0.2	5
R696E&D727R	670.2 ± 11.4	171.7 ± 5.6	-22.1 ± 0.4	5
R696D&D727K	604.8 ± 6.2	157.0 ± 2.5	-20.5 ± 0.1	5
R696D&D727R	1275.9 ± 39.8	274.5 ± 10.3	-23.0 ± 0.5	5
WT	723.5 ± 19.8	171.8 ± 5.2	-22.3 ± 1.2	5
D727K	365.4 ± 11.7	105.9 ± 3.5	-26.3 ± 0.6	5
D727R	570.7 ± 15.7	153.2 ± 4.6	-28.9 ± 0.4	5
R752E	165.6 ± 9.4	58.5 ± 2.1	-26.2 ± 0.7	5
R752D	149.0 ± 9.2	52.1 ± 1.6	-18.9 ± 0.8	5
D727K&R752E	823.6 ± 9.3	200.6 ± 3.9	38.1 ± 0.5	5
D727K&R752D	275.5 ± 8.0	91.7 ± 3.0	-21.5 ± 1.1	5
D727R&R752E	1215.2 ± 27.2	258.3 ± 12.0	-37.8 ± 0.3	5
D727R&R752D	365.9 ± 7.5	113.6 ± 3.0	-22.4 ± 0.5	5
WT---WT	450.7 ± 22.1	89.9 ± 5.5	-	5
R696E---D767K	397.7 ± 28.4	71.7 ± 2.3	-	5
R696E&D767K---WT	595.8 ± 33.4	111.2 ± 4.2	-	5
R696E&D767K---R696E&D76	892.2 ± 33.3	166.0 ± 6.1	-	5
WT---WT	455.0 ± 26.4	92.6 ± 7.4	-	5
D727K---R752E	219.2 ± 40.9	48.0 ± 4.2	-	5
D727K&R752E---WT	417.7 ± 21.0	92.3 ± 4.5	-	5
D727K&R752E---D727K&R75	457.3 ± 17.6	98.8 ± 2.7	-	5

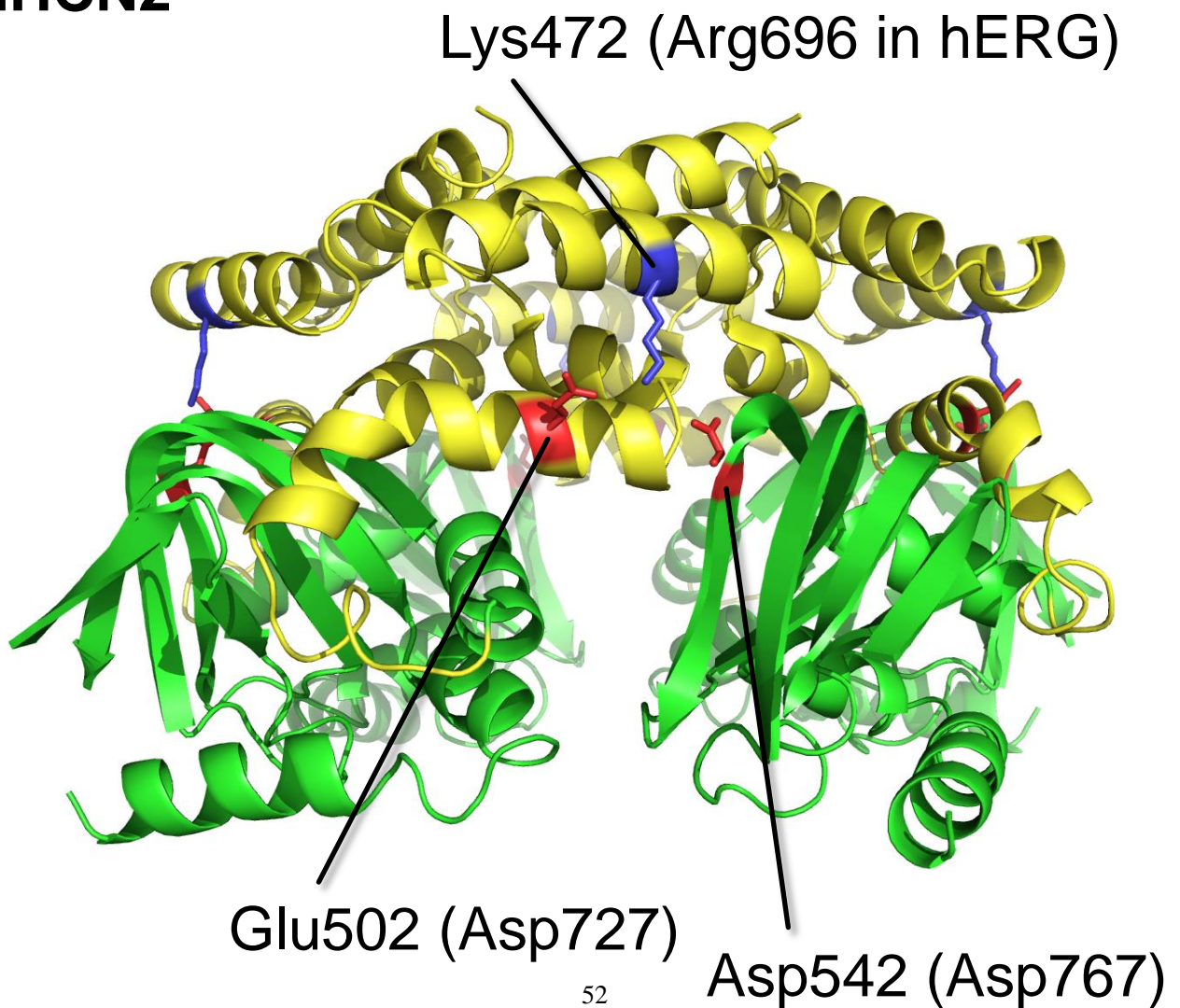
Each value shows Mean ± SEM.

A



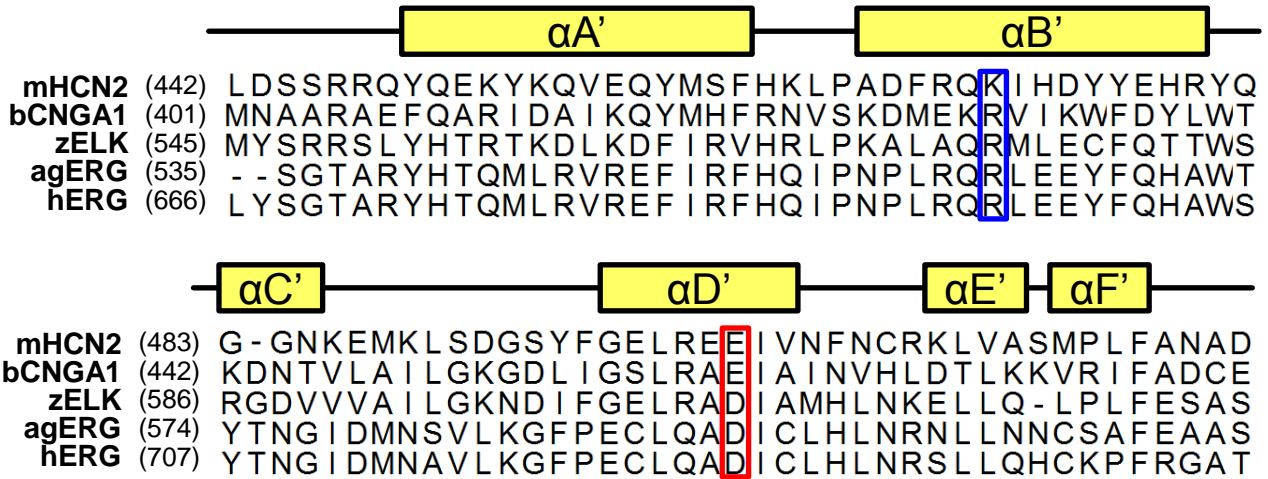
B

mHCN2



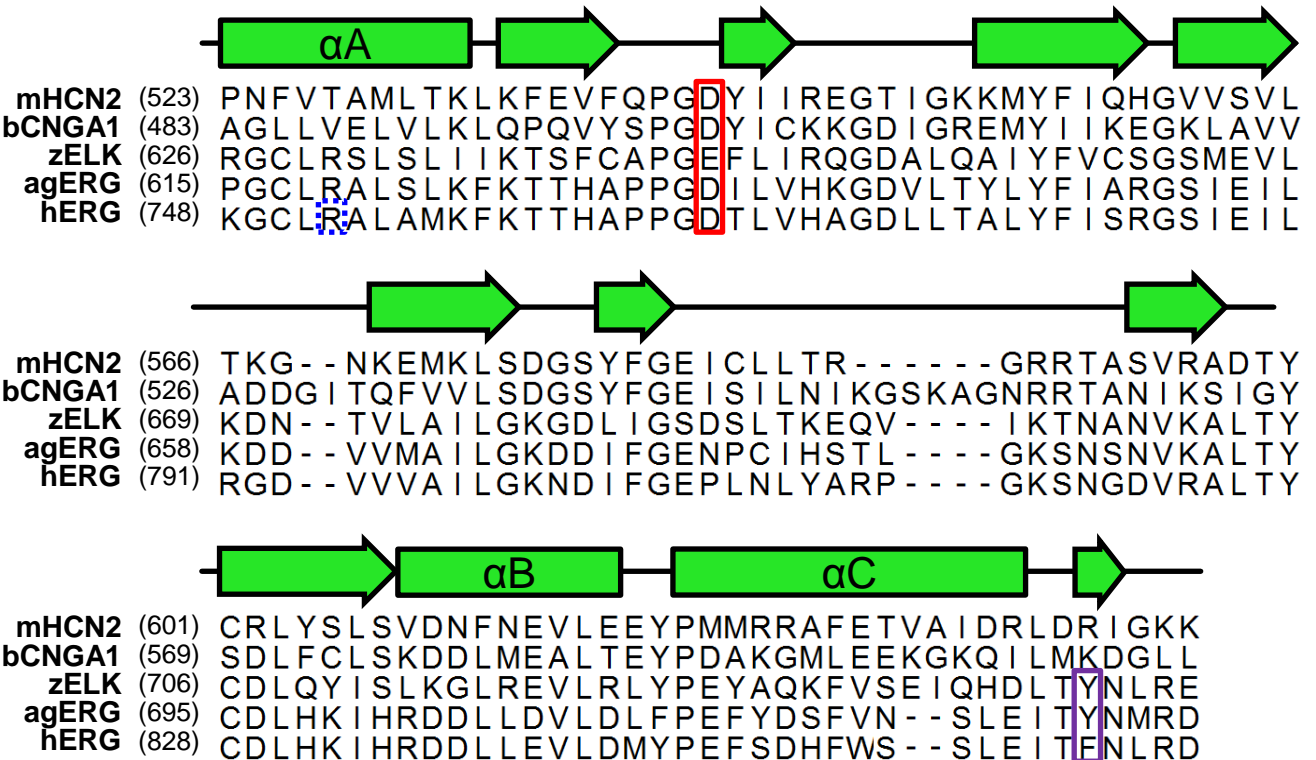
A

## C-linker domain

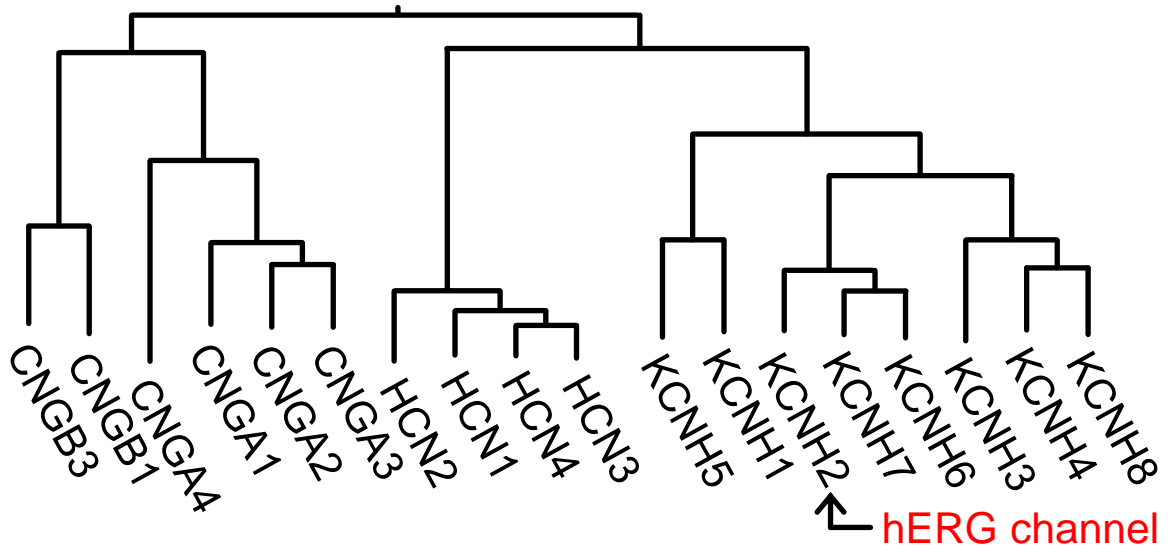


B

## CNB domain

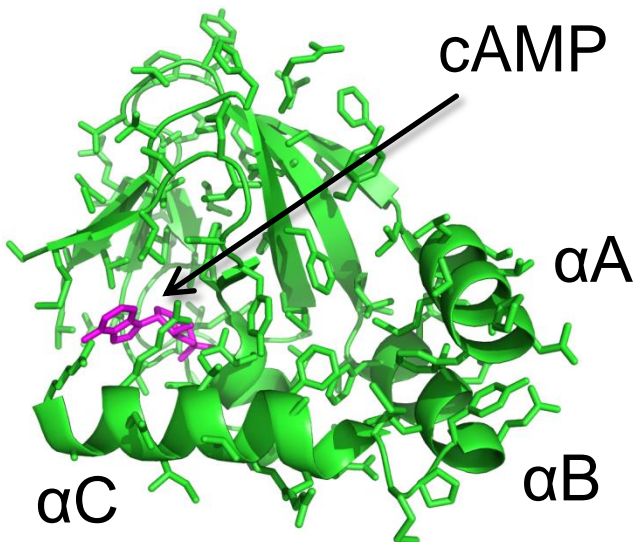


**A**

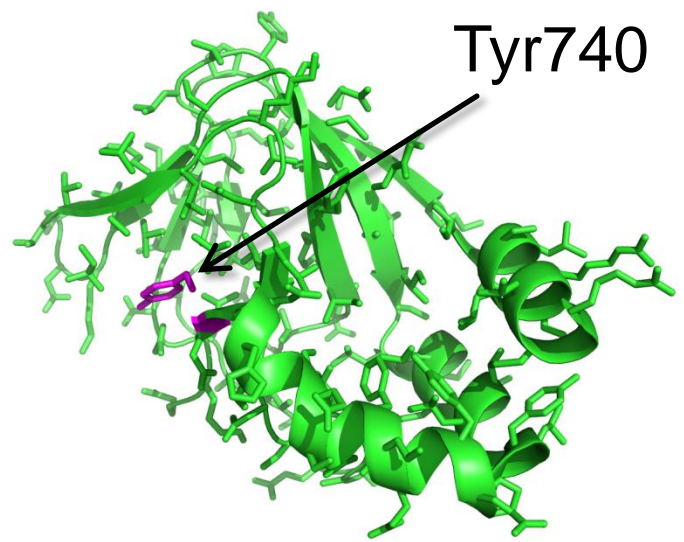


**B**

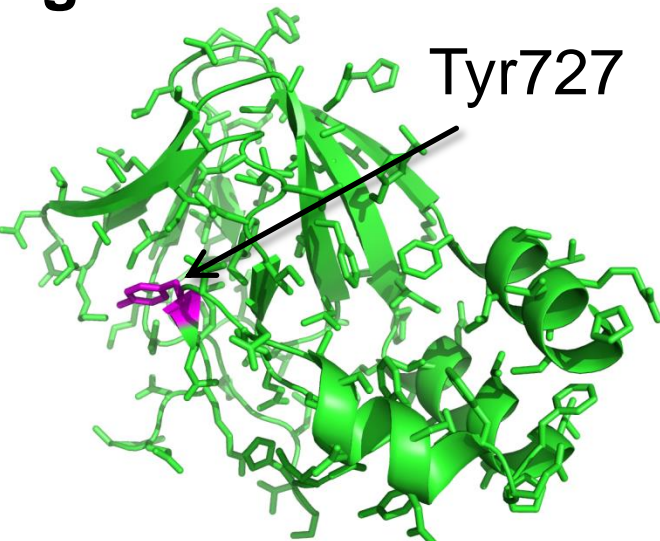
**mHCN2**



**zELK**



**agERG**



**hERG1a (Modeling)**

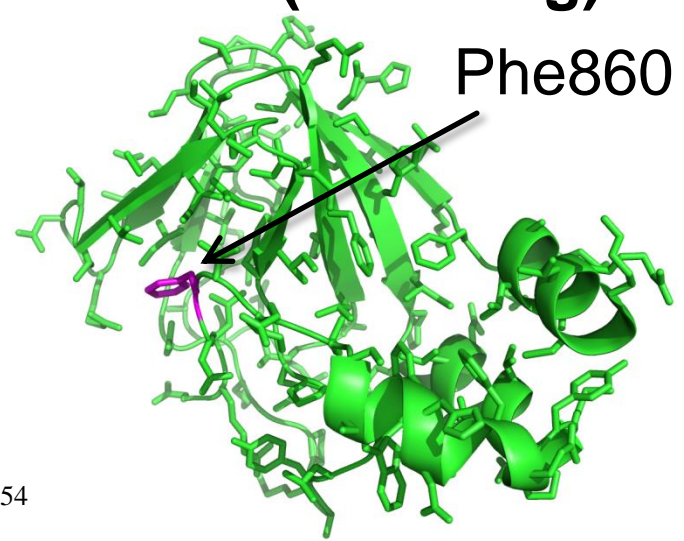
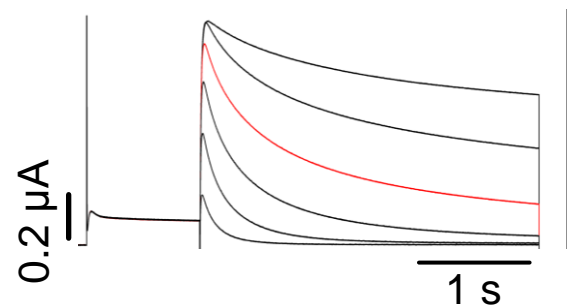


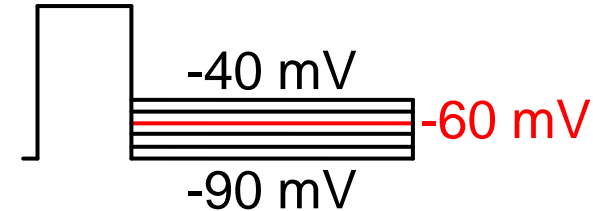
Figure 4

**A**

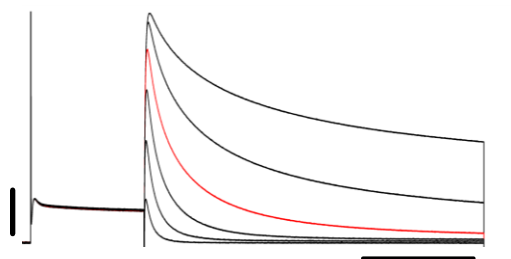
● WT



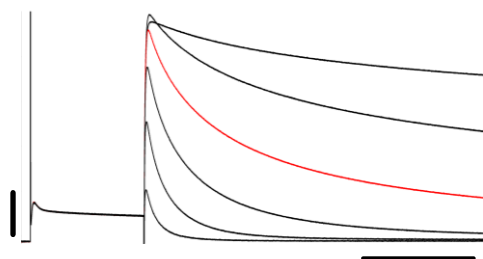
40 mV



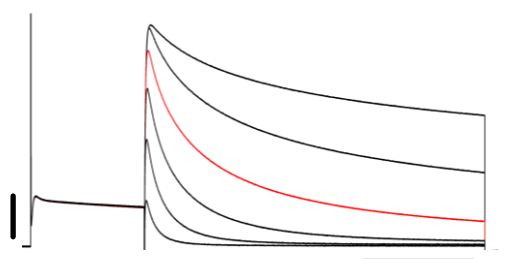
■ F860A



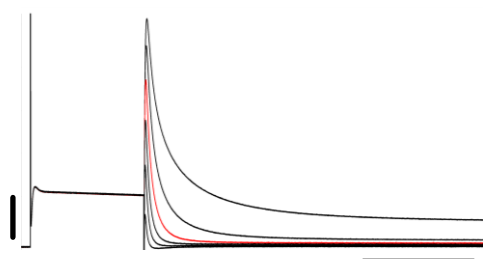
► F860V



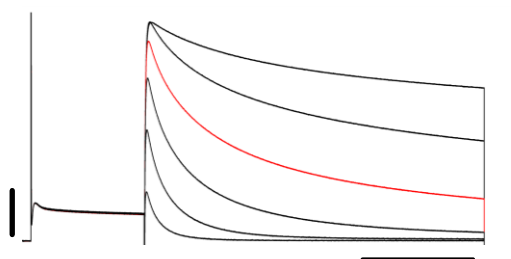
▲ F860Y



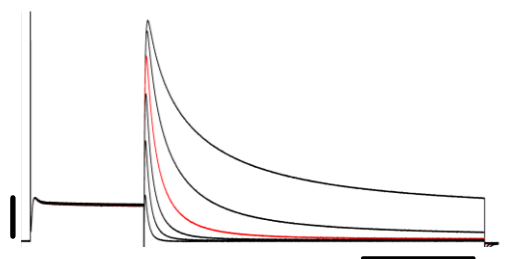
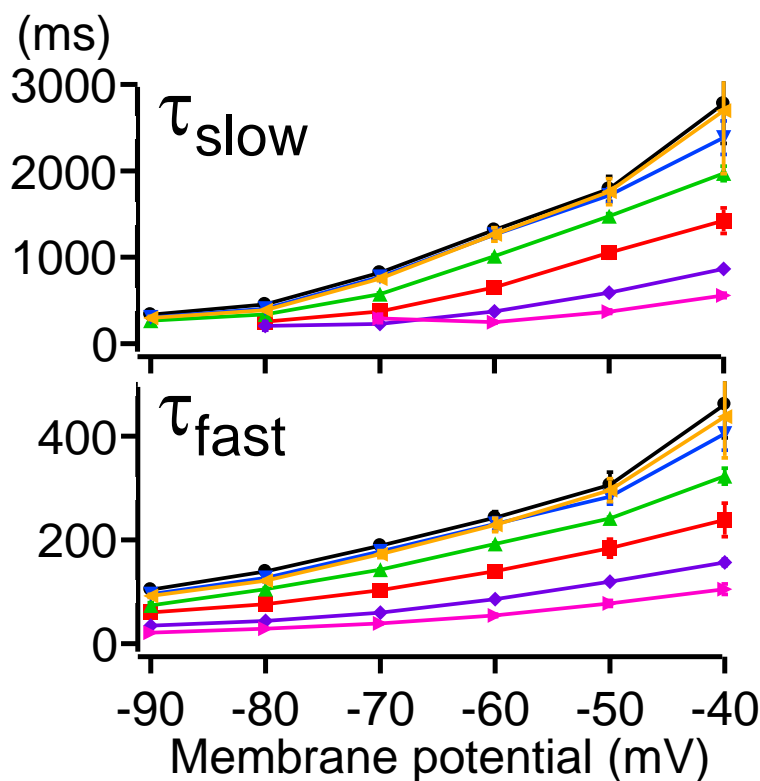
◄ F860E



▼ F860I

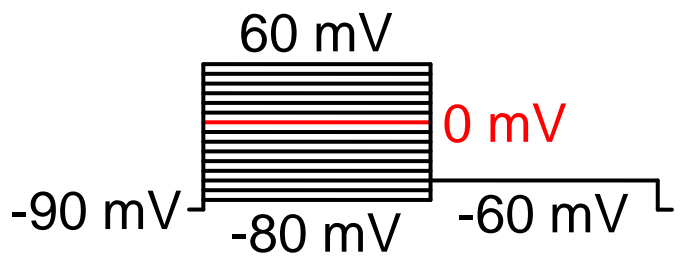
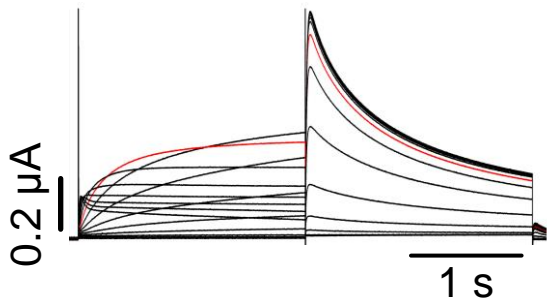


◆ F860R

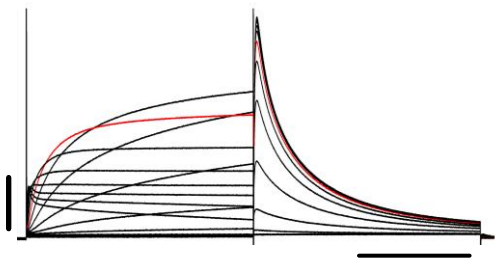
**B**

A

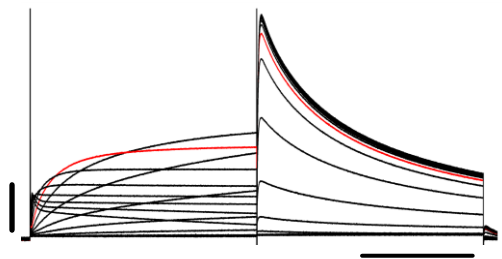
● WT



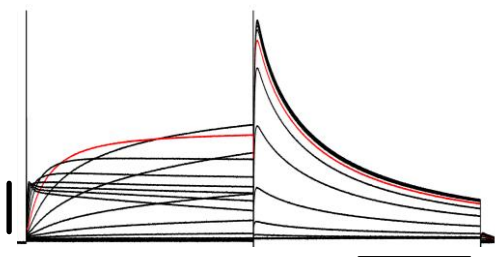
■ F860A



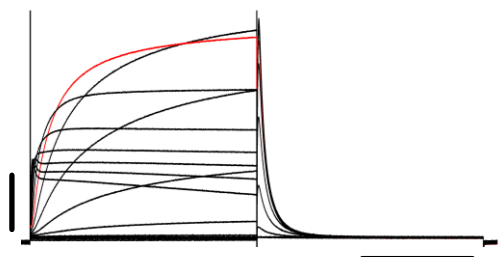
► F860V



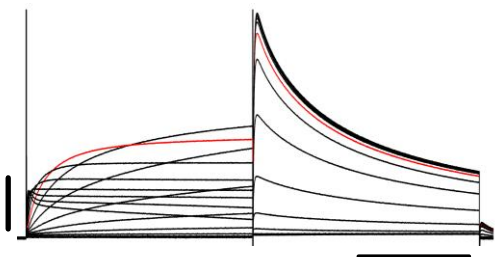
▲ F860Y



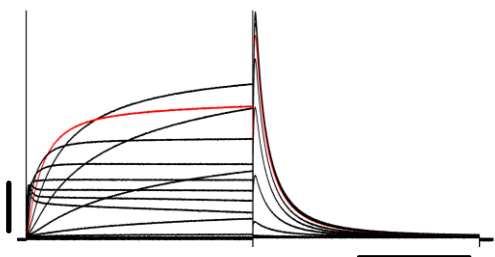
◄ F860E



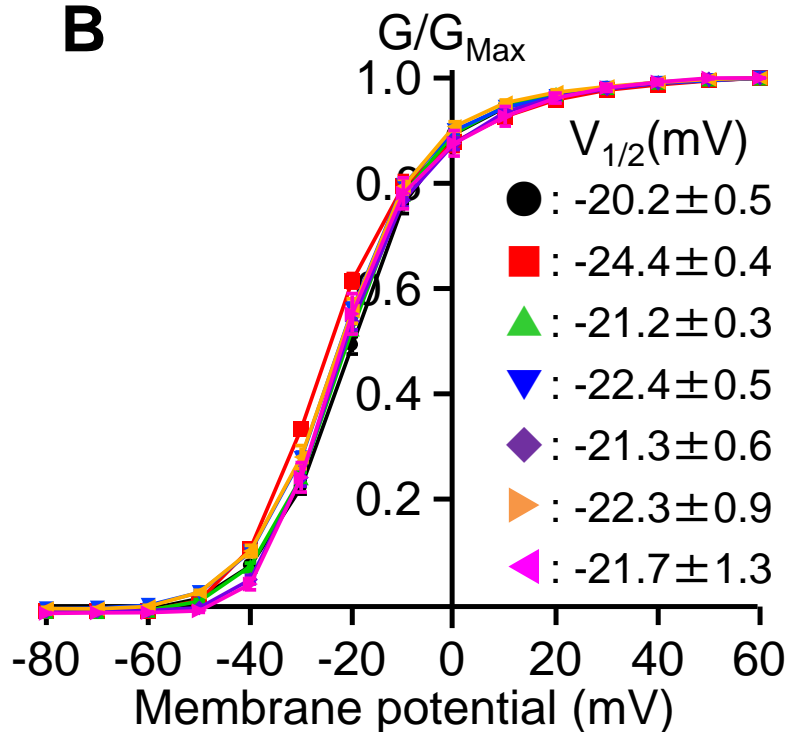
▼ F860I



◆ F860R



B



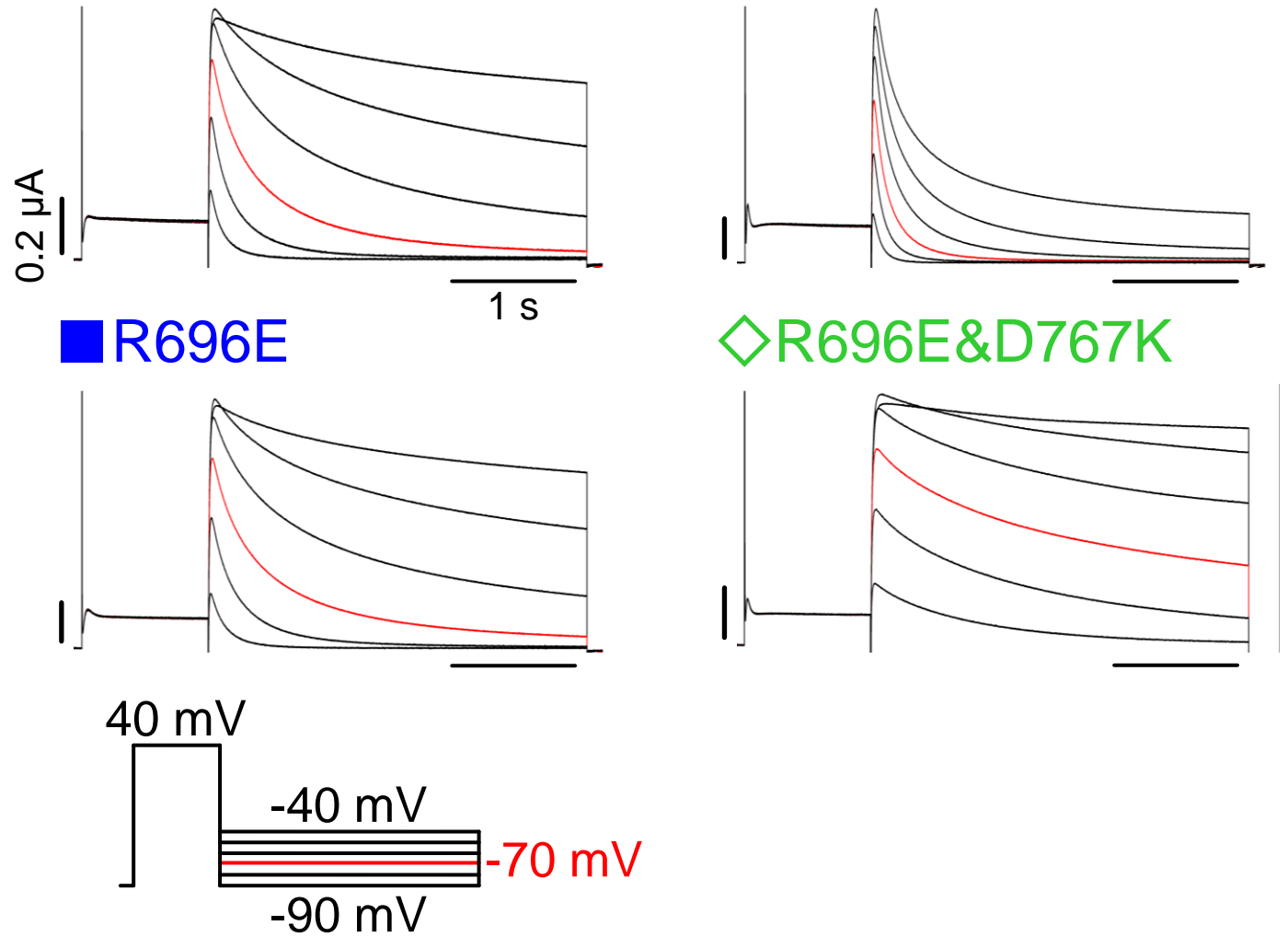
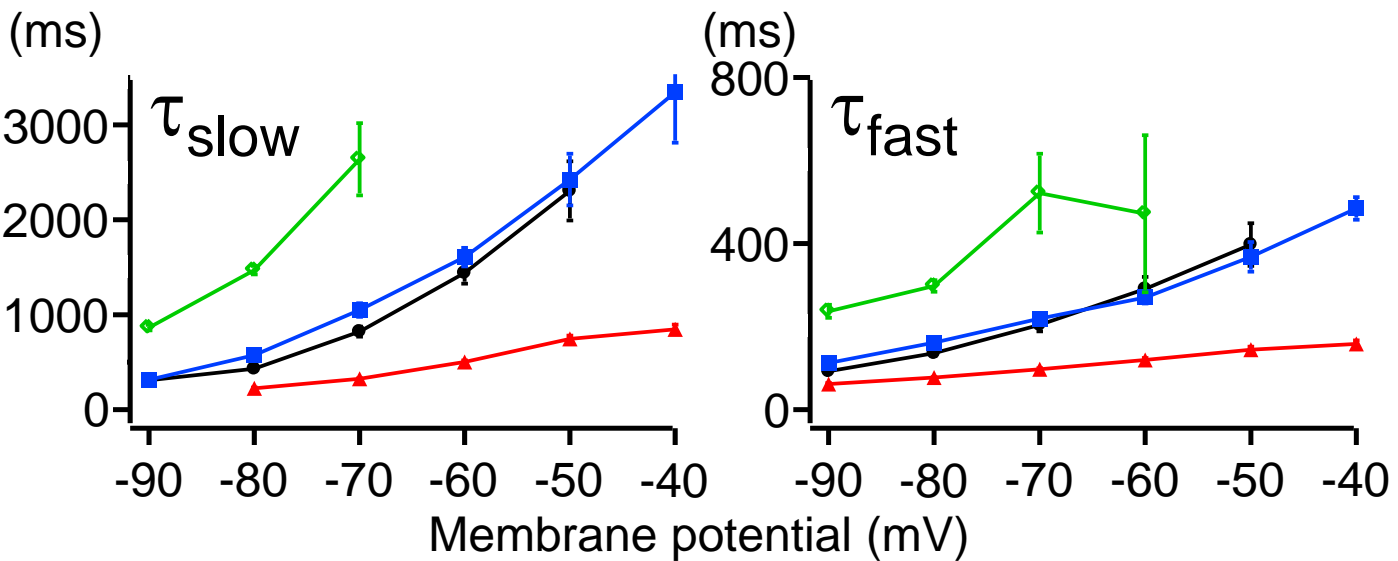
**A**

● WT

▲ D767K

■ R696E

◇ R696E&amp;D767K

**B**

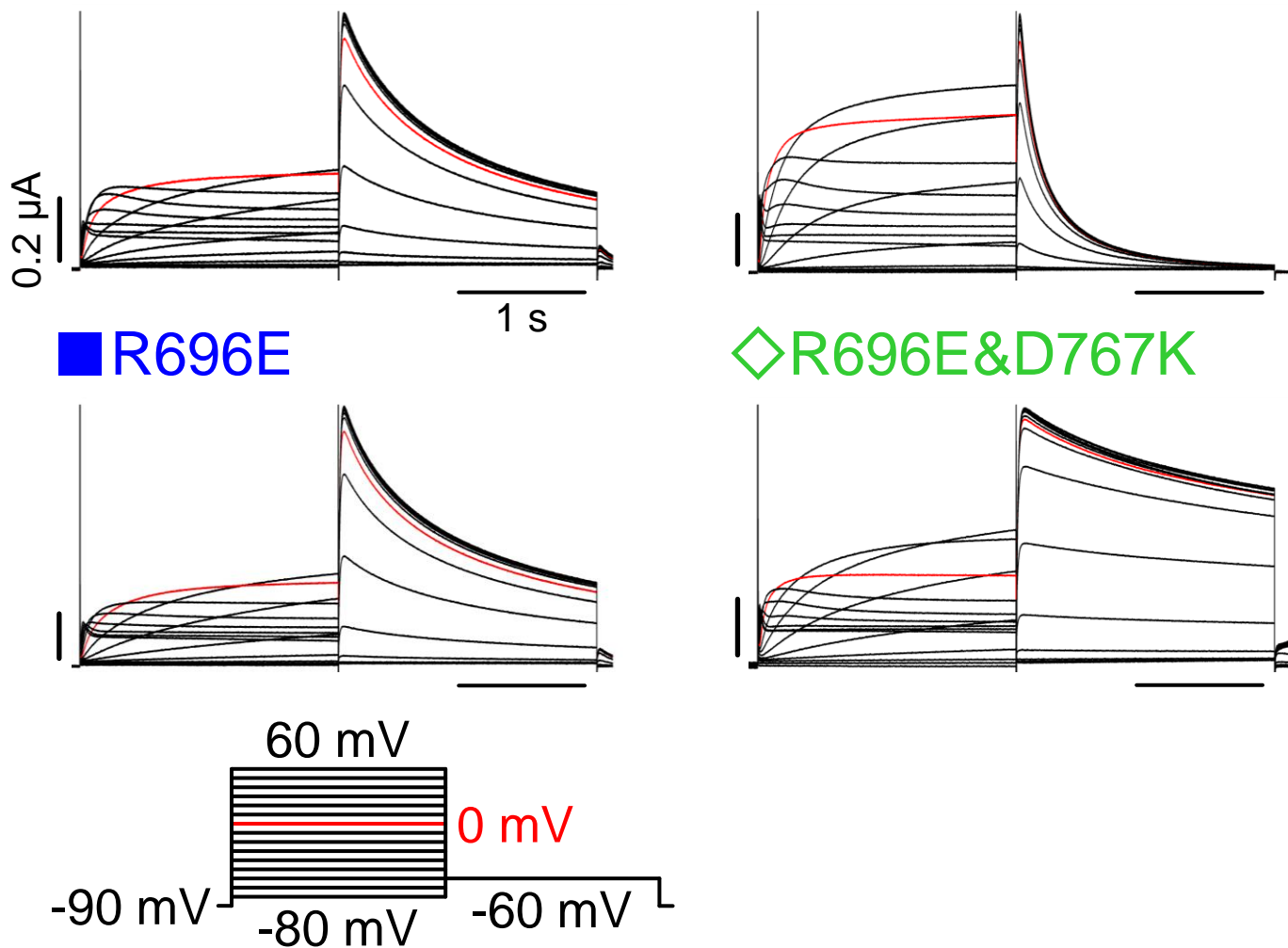
A

● WT

▲ D767K

■ R696E

◇ R696E&amp;D767K



B

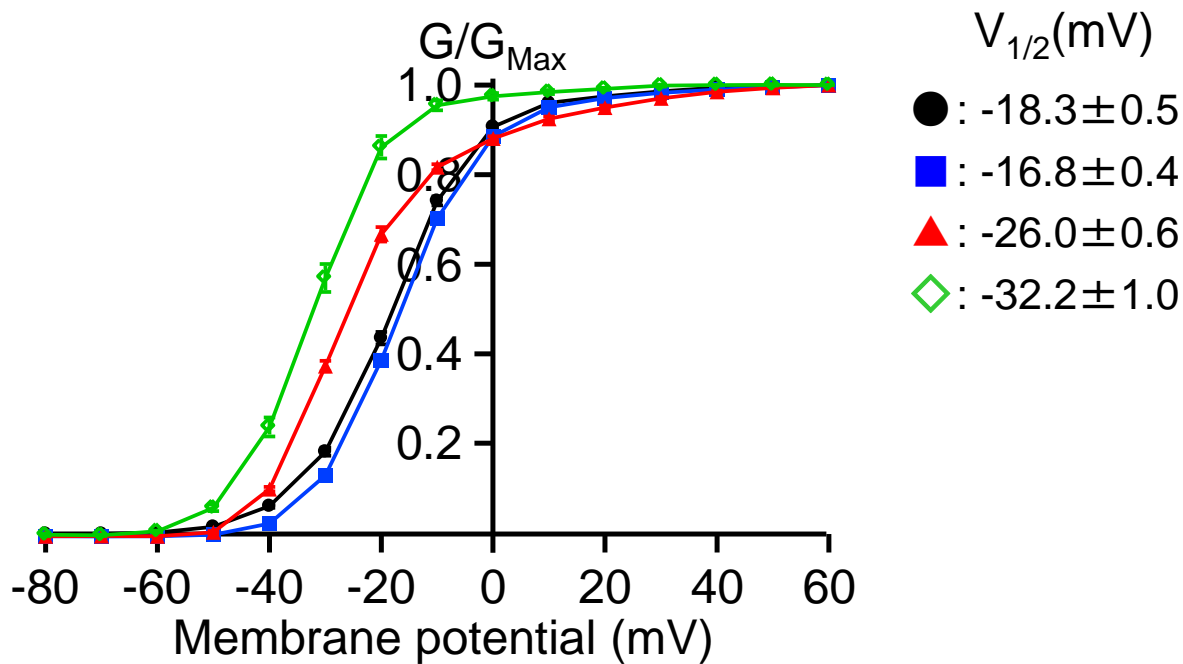
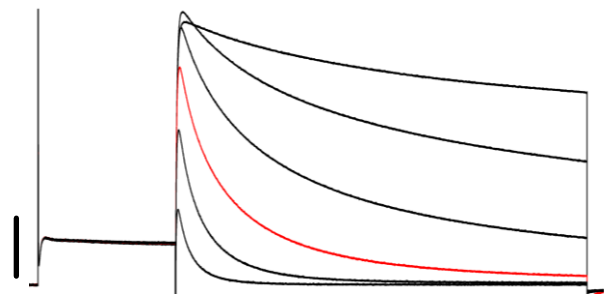


Figure 8

**A**

● WT



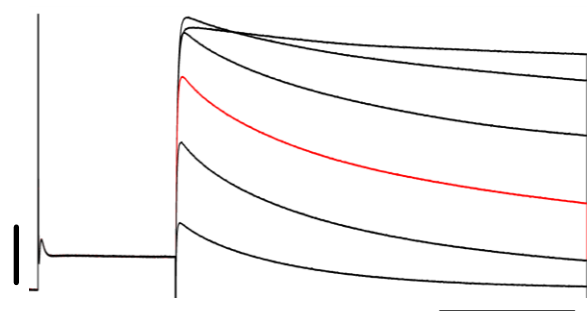
40 mV

-40 mV

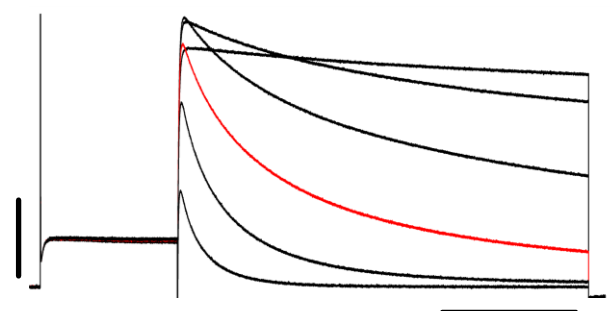
-90 mV

-70 mV

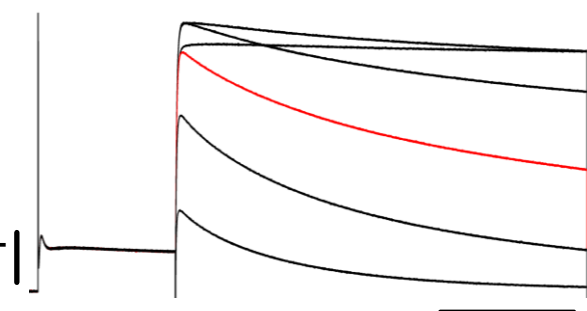
◇ R696E&D767K



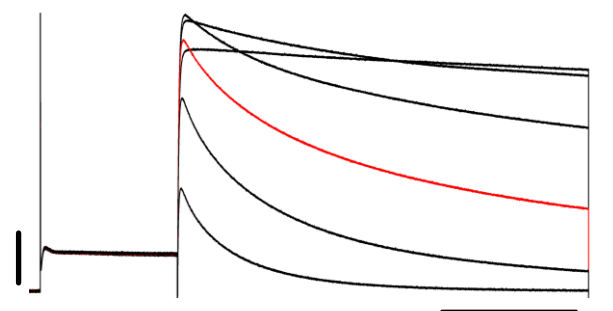
◇ R696E&D767R



◇ R696D&D767K



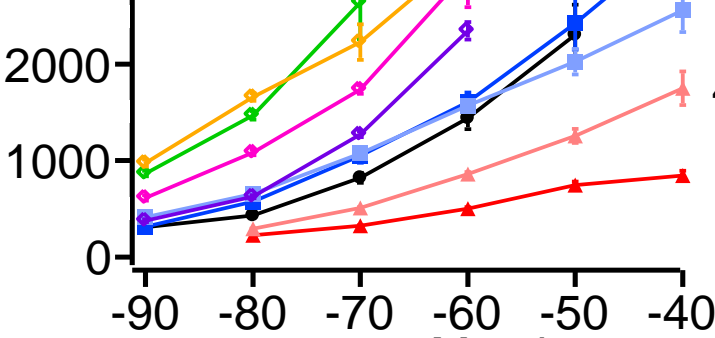
◇ R696D&D767R



**B**

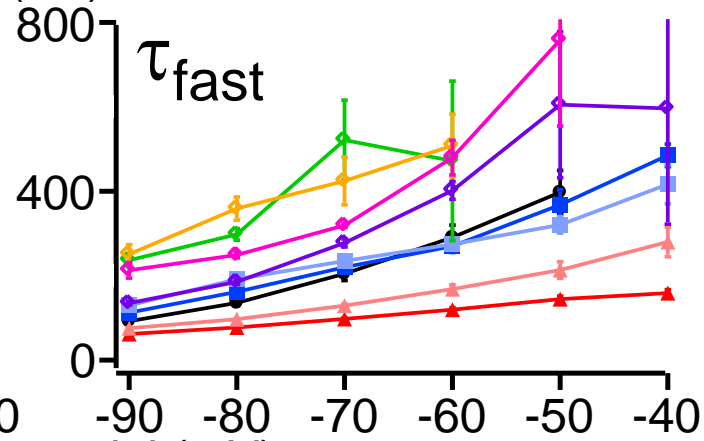
(ms)

$\tau_{slow}$



(ms)

$\tau_{fast}$



Membrane potential (mV)

■ R696E

■ R696D

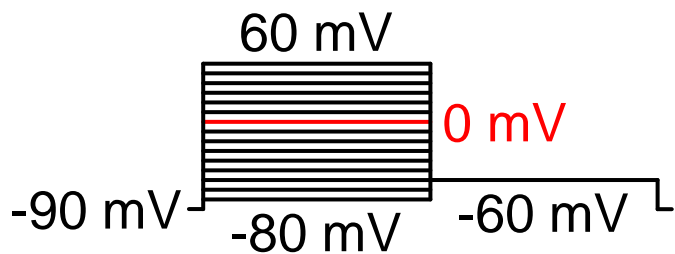
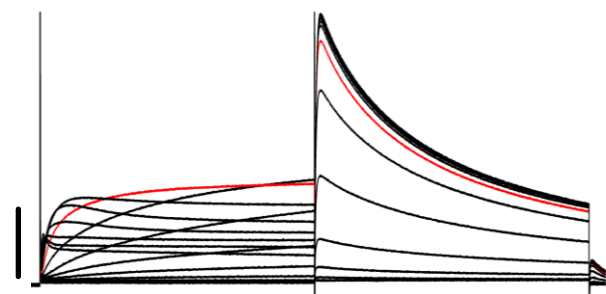
▲ D767K

▲ D767R

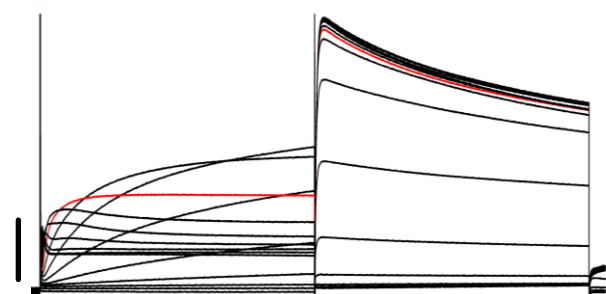
Figure 9

**A**

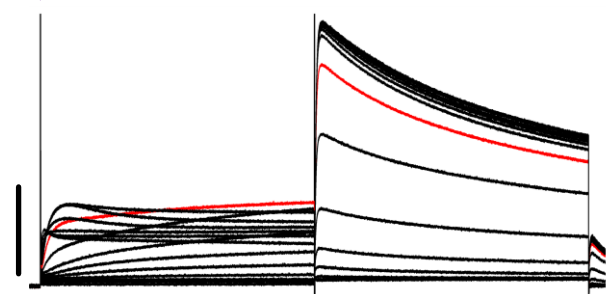
● WT



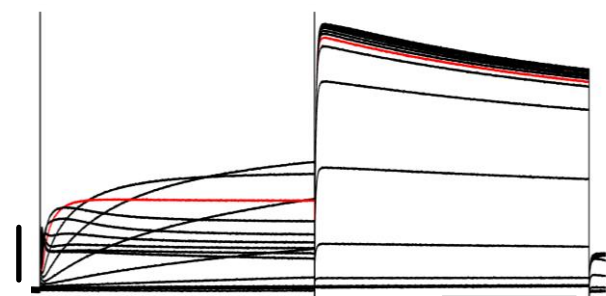
◇ R696E&D767K



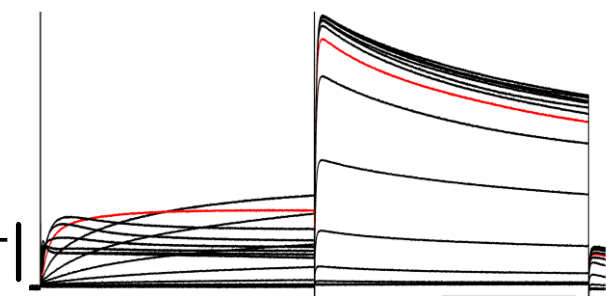
◇ R696E&D767R



◇ R696D&D767K



◇ R696D&D767R



0.2  $\mu$ A

1 s

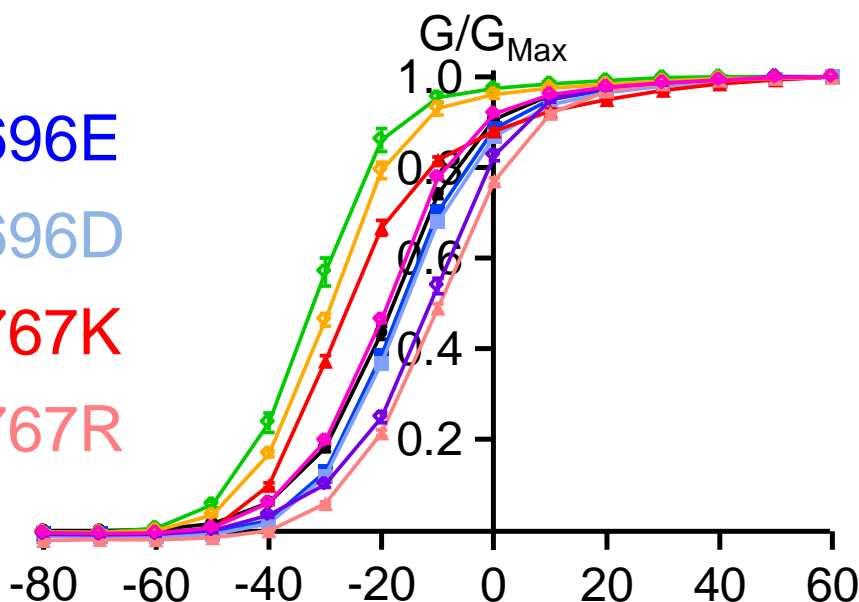
**B**

■ R696E

■ R696D

▲ D767K

▲ D767R



$V_{1/2}$  (mV)

● :  $-18.3 \pm 0.5$

■ :  $-16.8 \pm 0.4$

■ :  $-16.2 \pm 0.3$

▲ :  $-26.0 \pm 0.6$

▲ :  $-10.2 \pm 0.3$

◇ :  $-32.2 \pm 1.0$

◇ :  $-11.7 \pm 0.5$

◇ :  $-29.3 \pm 0.5$

◇ :  $-19.5 \pm 0.2$

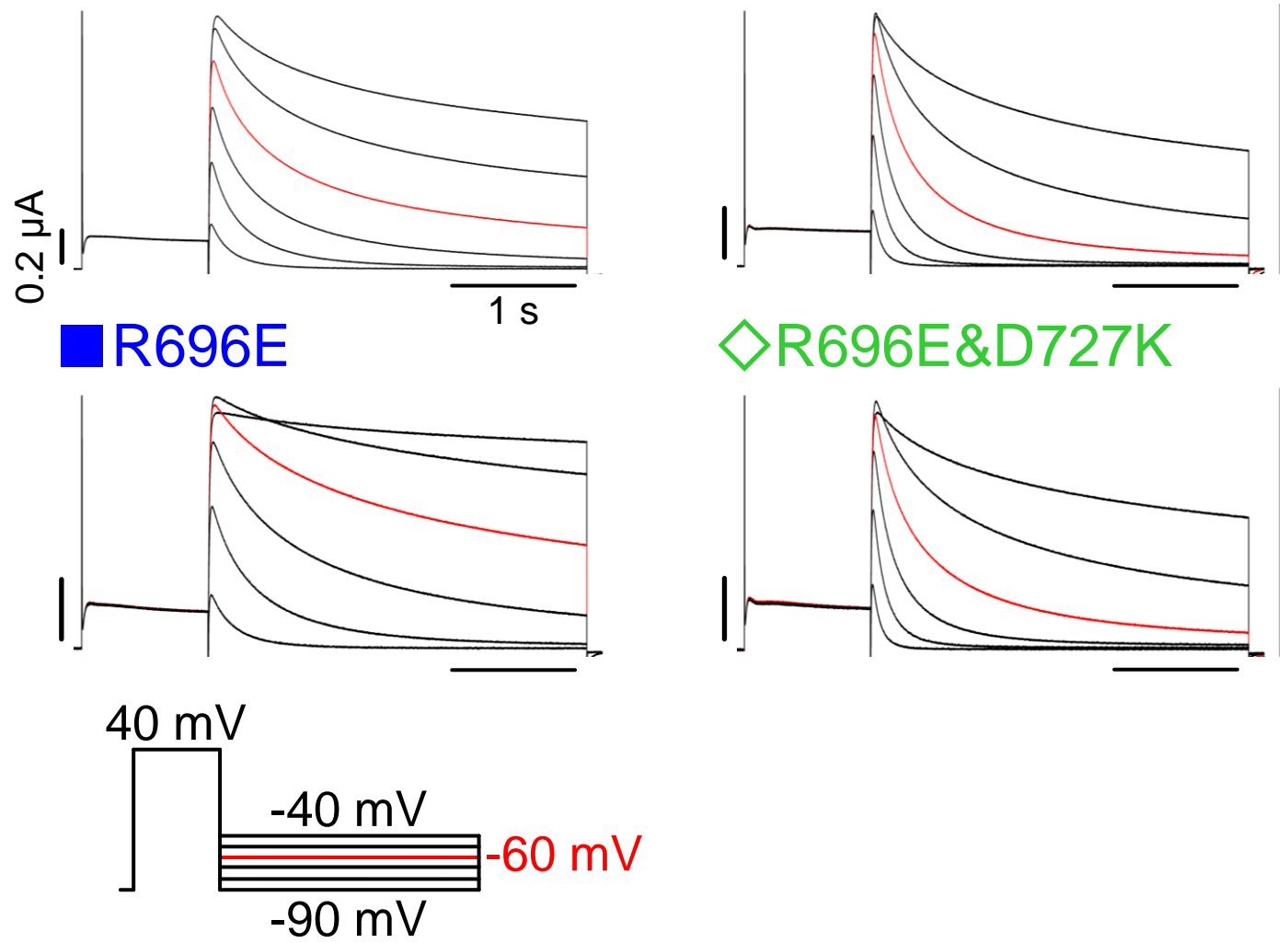
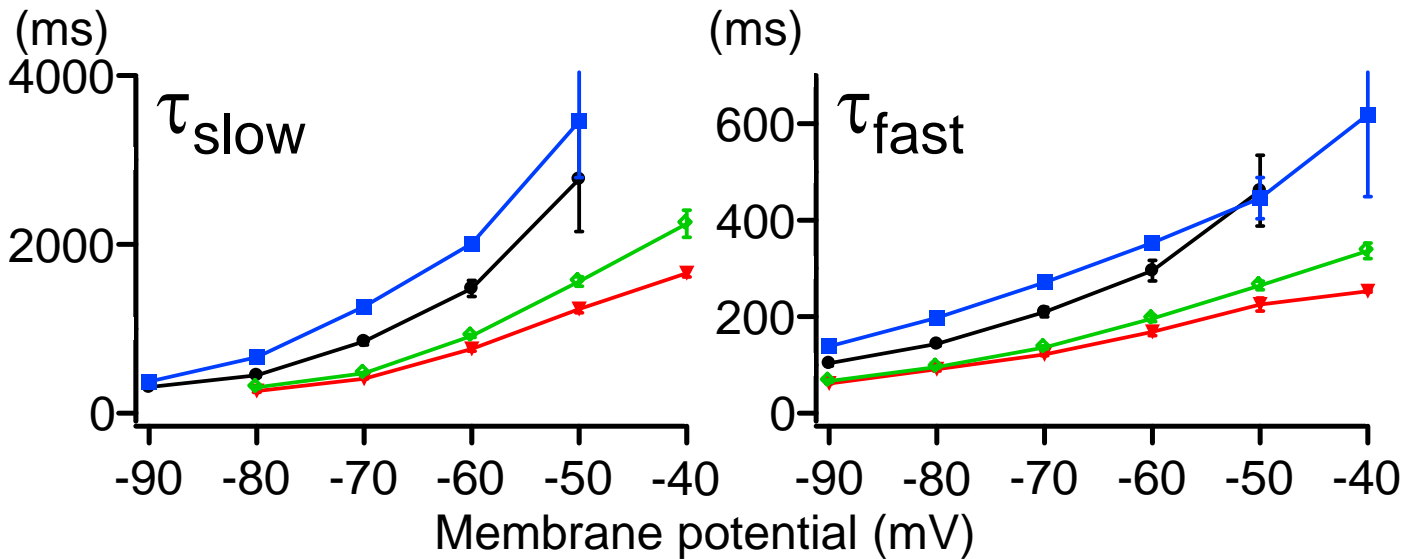
**A**

● WT

▼ D727K

■ R696E

◇ R696E&amp;D727K

**B**

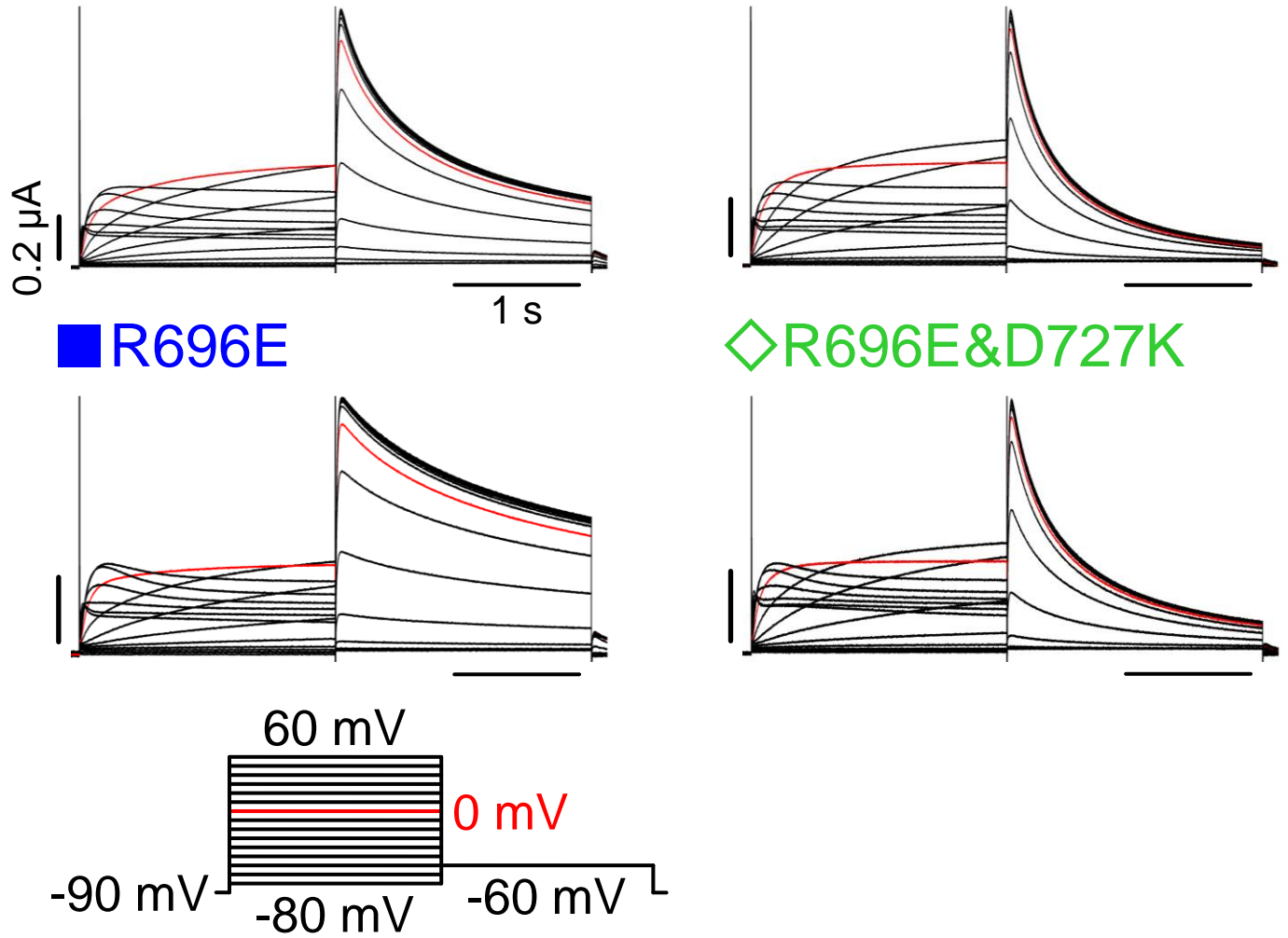
A

● WT

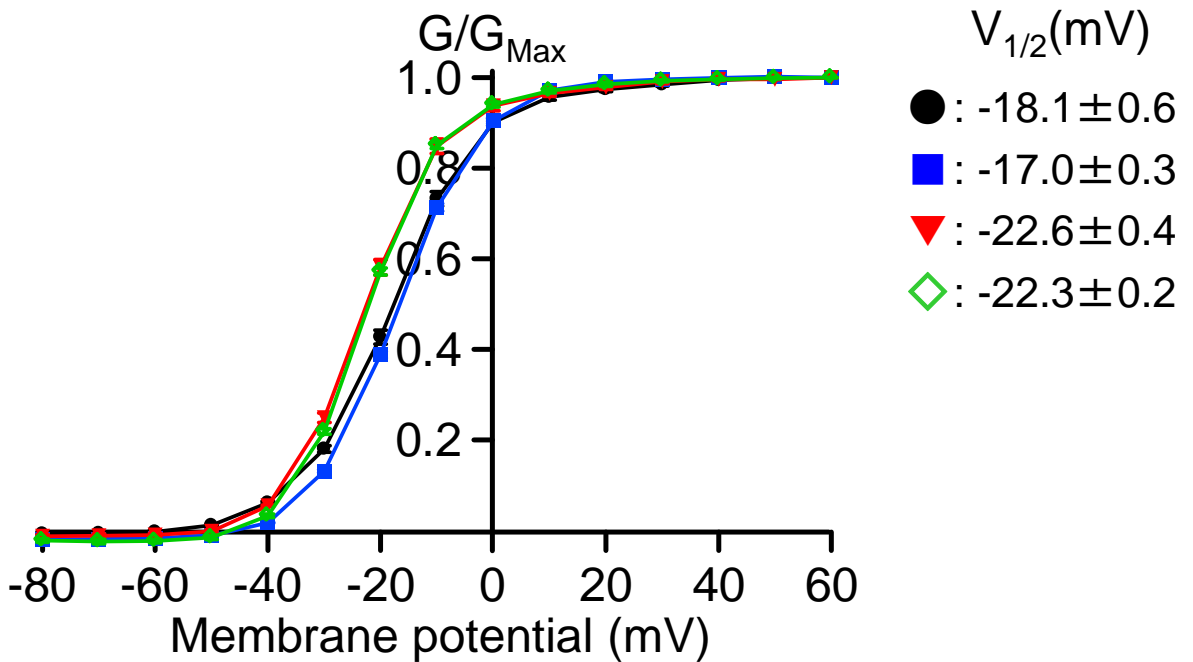
▼ D727K

■ R696E

◇ R696E&amp;D727K

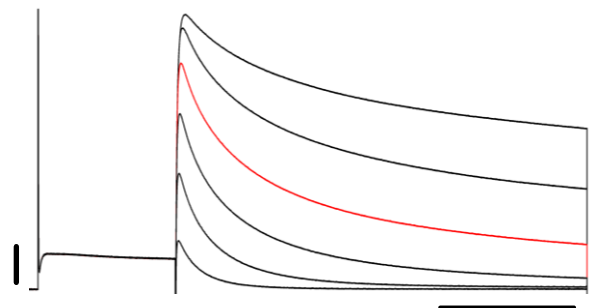


B



**A**

● WT



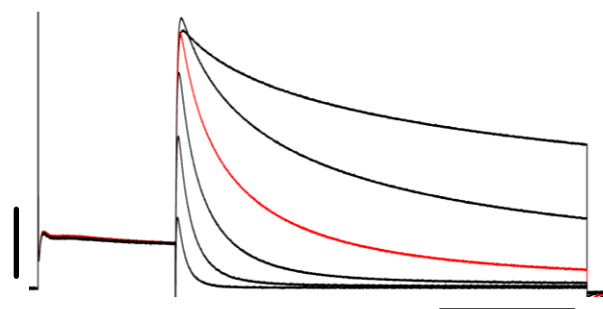
40 mV

-40 mV

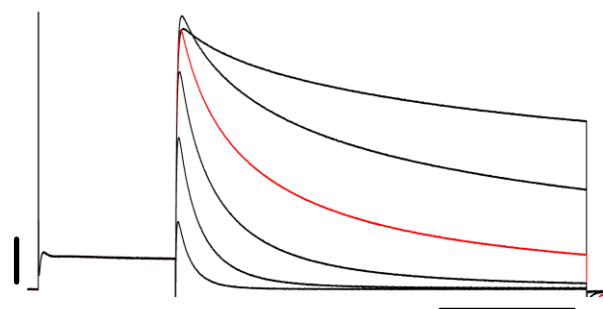
-90 mV

-60 mV

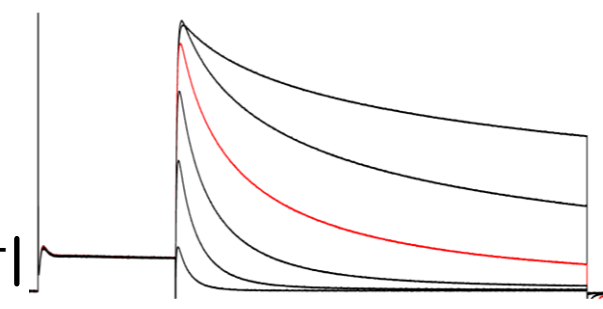
◇ R696E&amp;D727K



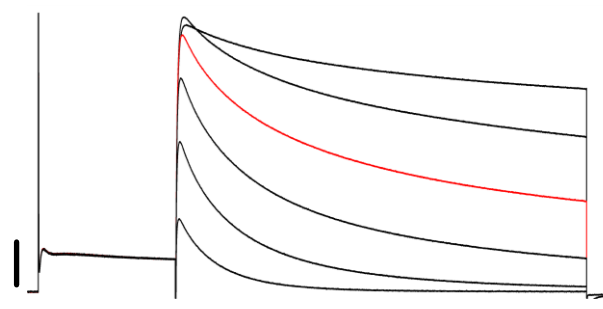
◇ R696E&amp;D727R



◇ R696D&amp;D727K



◇ R696D&amp;D727R

0.2  $\mu$ A

1 s

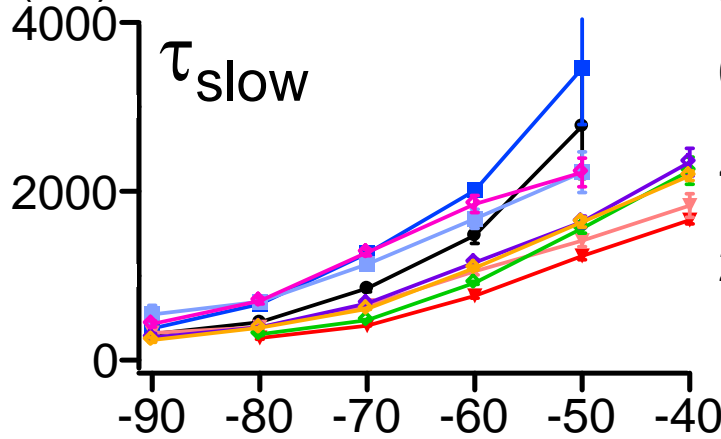
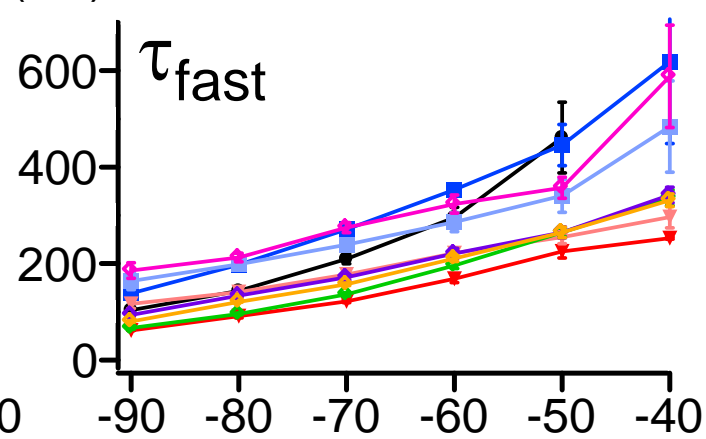
**B**

■ R696E

■ R696D

(ms) ▲ D727K

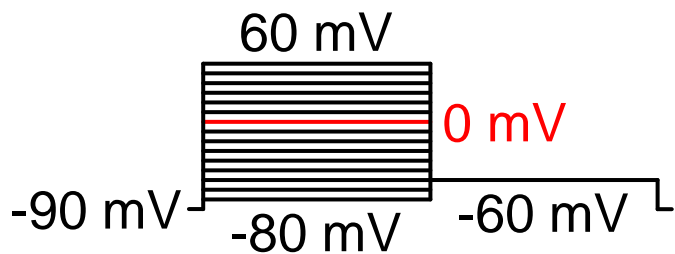
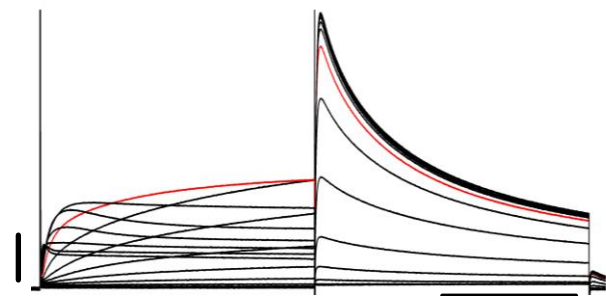
▲ D727R

 $\tau_{\text{slow}}$  $\tau_{\text{fast}}$ 

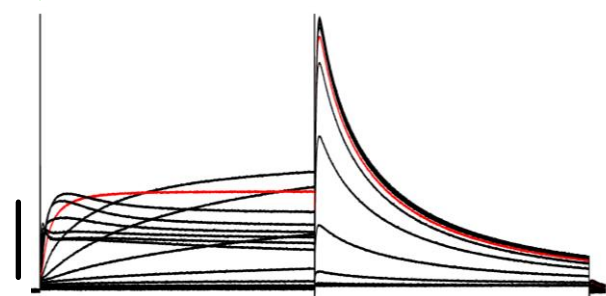
Membrane potential (mV)

**A**

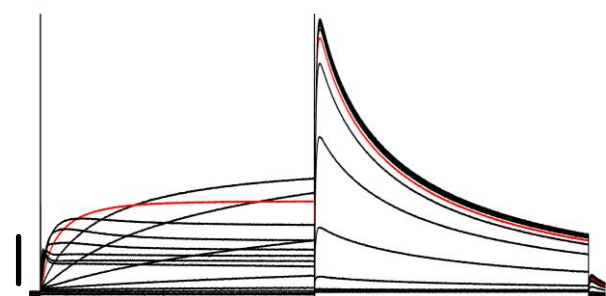
● WT



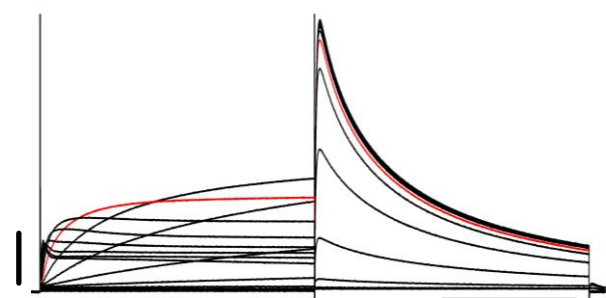
◇ R696E&D727K



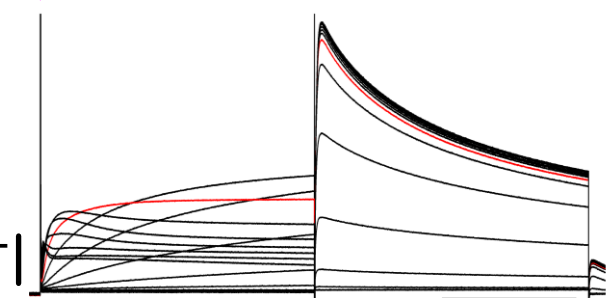
◇ R696E&D727R



◇ R696D&D727K



◇ R696D&D727R



0.2  $\mu$ A

1 s

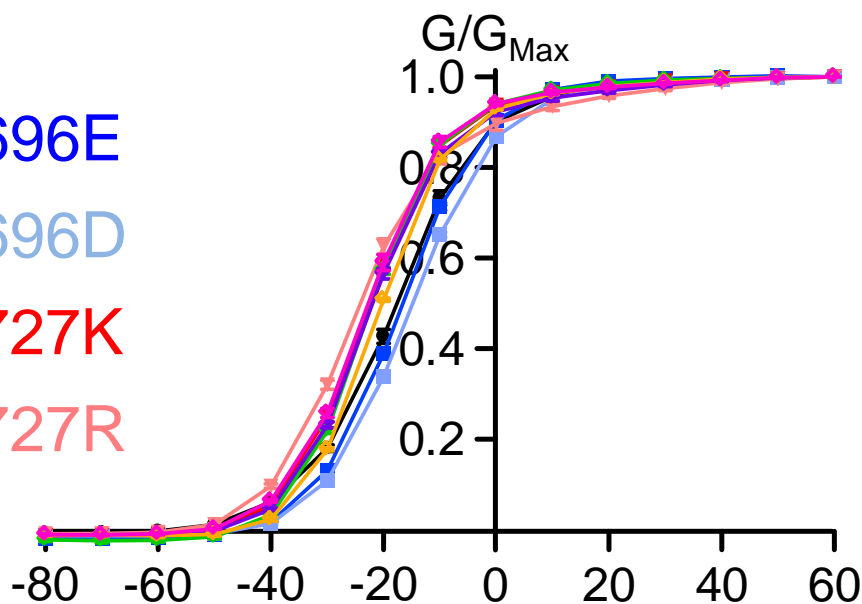
**B**

■ R696E

■ R696D

▼ D727K

▼ D727R



$V_{1/2}$  (mV)

● :  $-18.1 \pm 0.6$

■ :  $-17.0 \pm 0.3$

■ :  $-15.1 \pm 0.2$

▼ :  $-22.6 \pm 0.4$

▼ :  $-24.4 \pm 0.6$

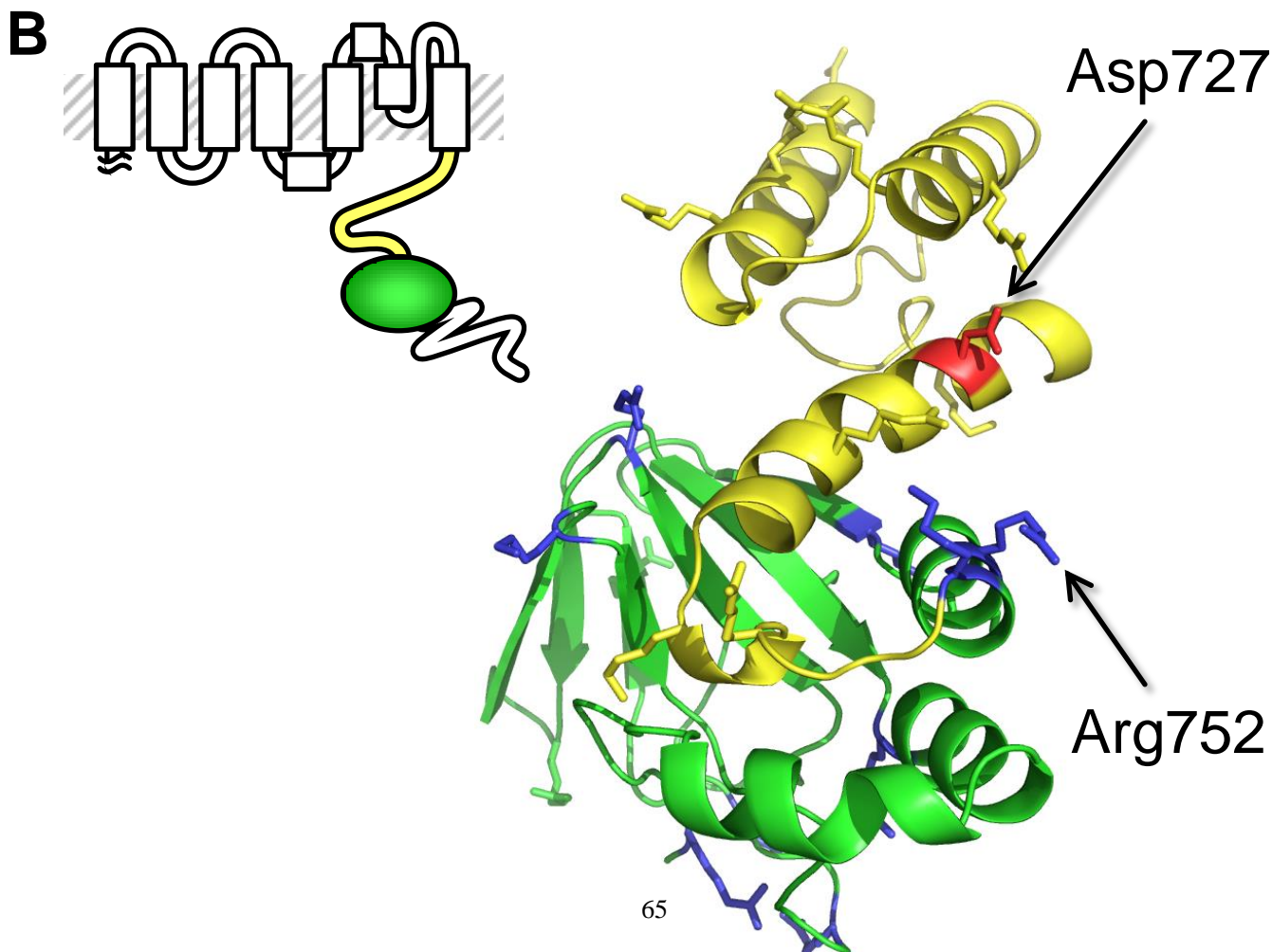
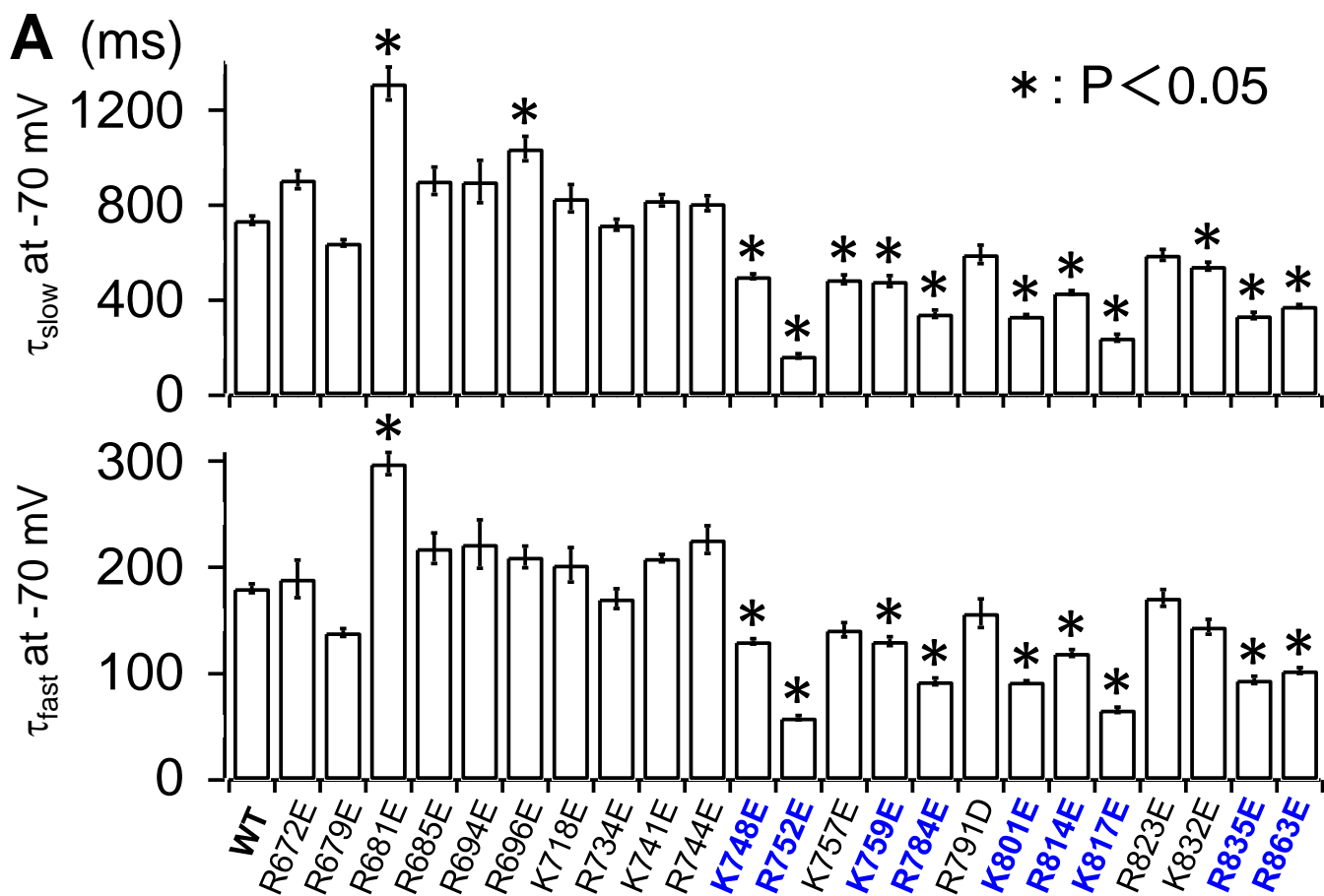
◇ :  $-22.3 \pm 0.2$

◇ :  $-22.1 \pm 0.4$

◇ :  $-20.5 \pm 0.1$

◇ :  $-23.0 \pm 0.5$

Figure 14



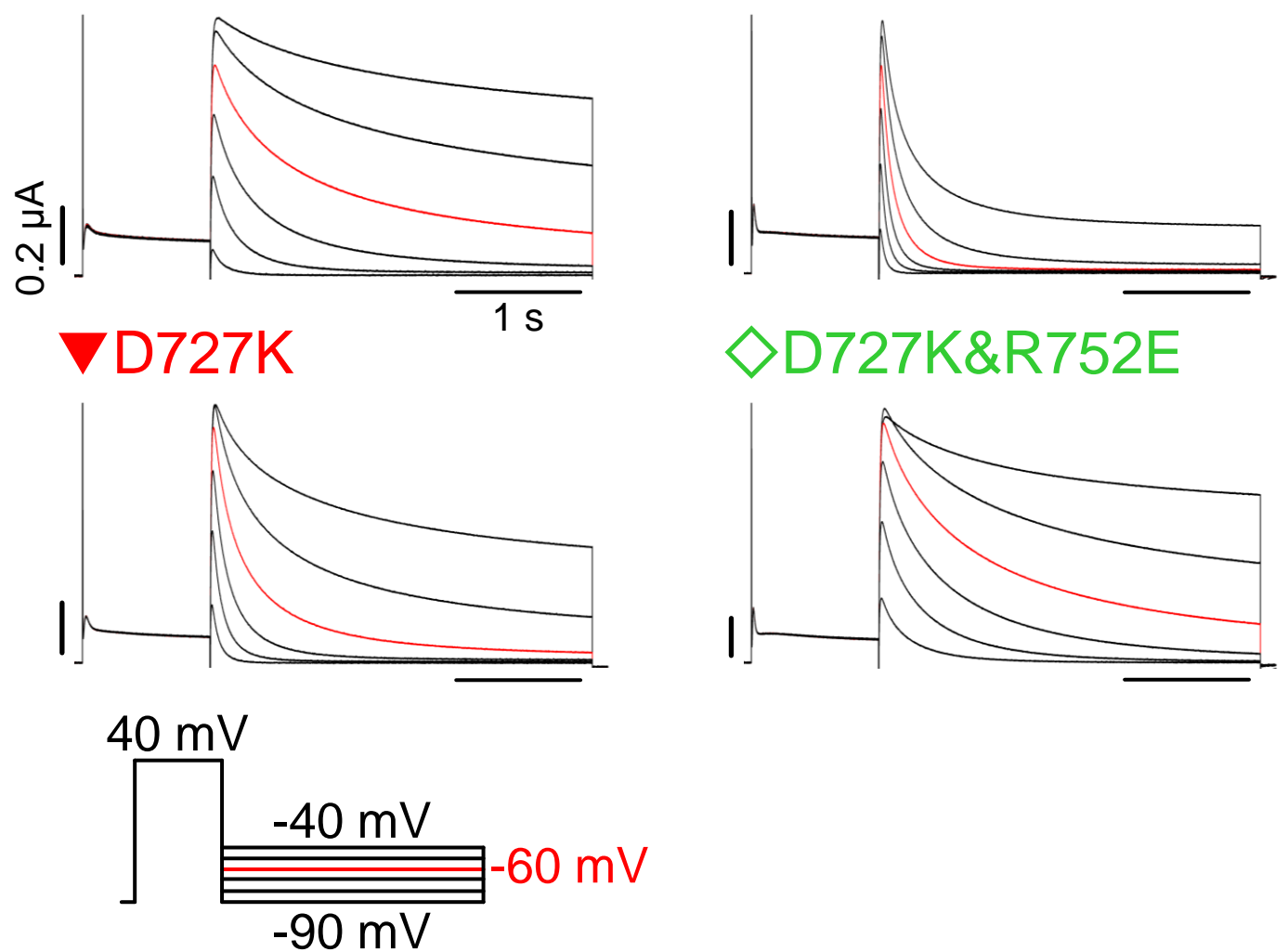
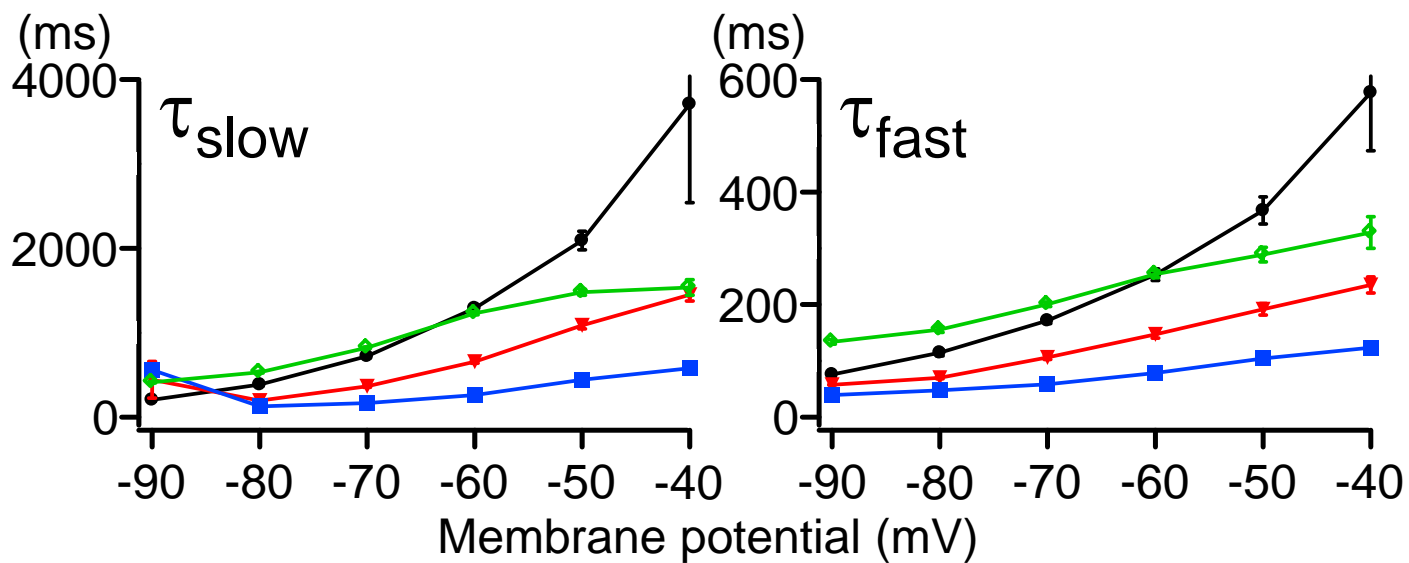
**A**

● WT

■ R752E

▼ D727K

◇ D727K&amp;R752E

**B**

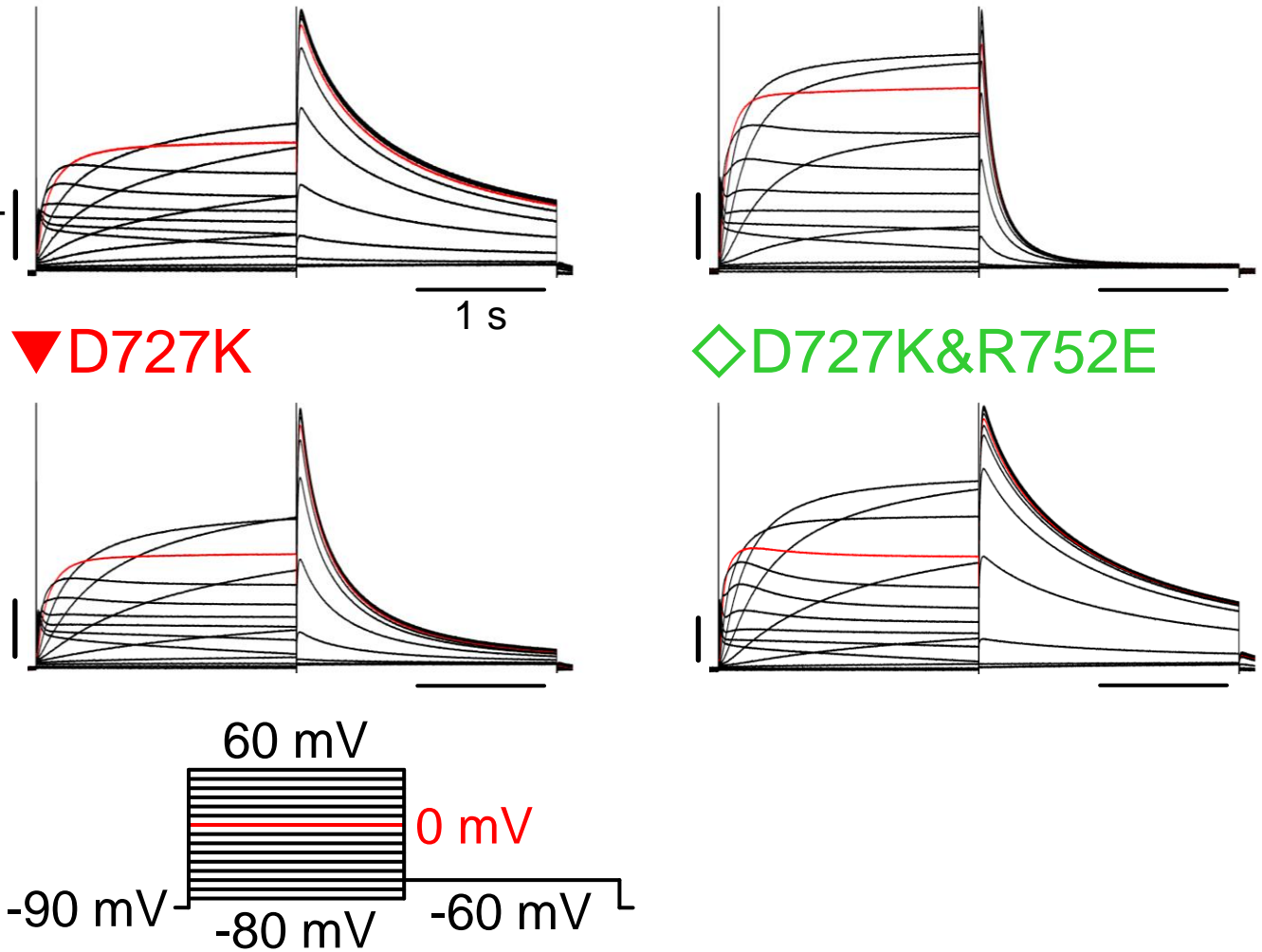
A

● WT

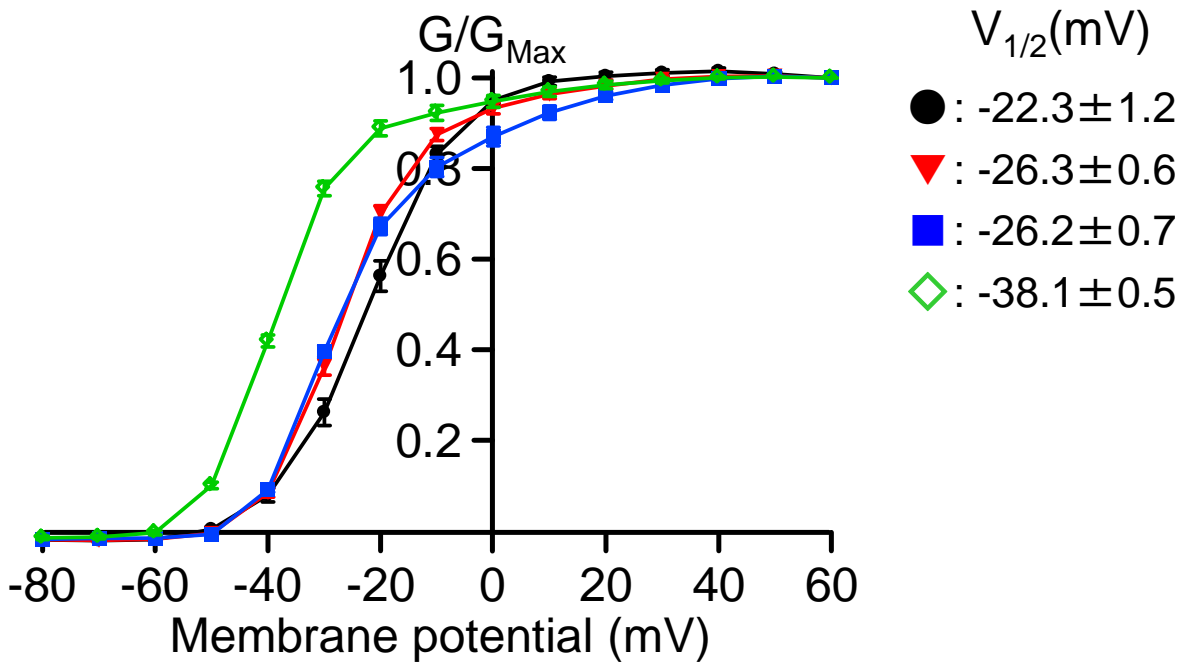
■ R752E

▼ D727K

◇ D727K&amp;R752E

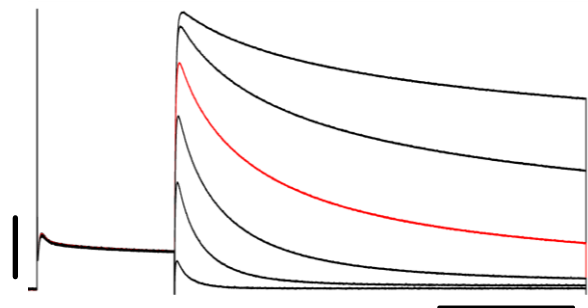


B



**A**

● WT

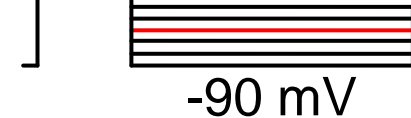


40 mV

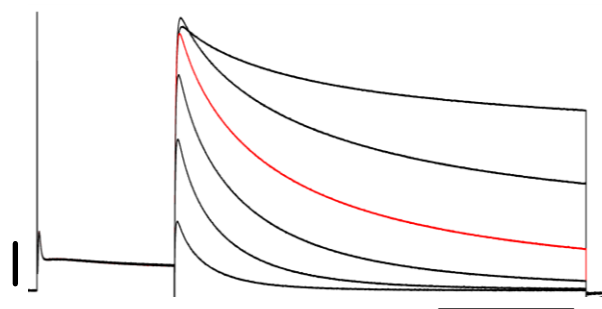
-40 mV

-90 mV

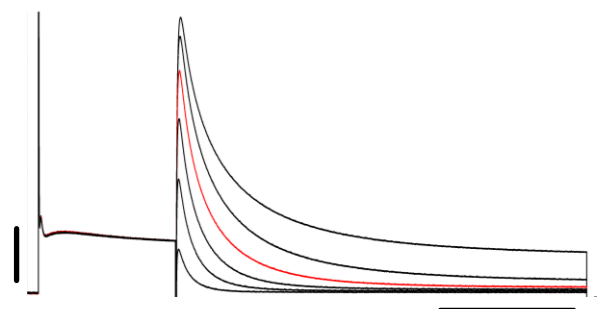
-60 mV



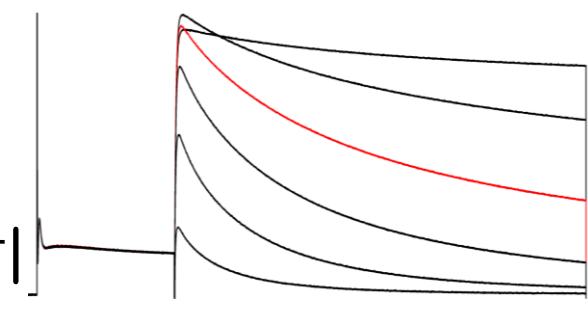
◇ D727K&amp;R752E



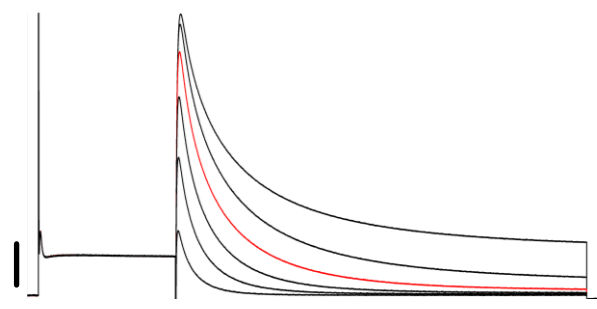
◇ D727K&amp;R752D



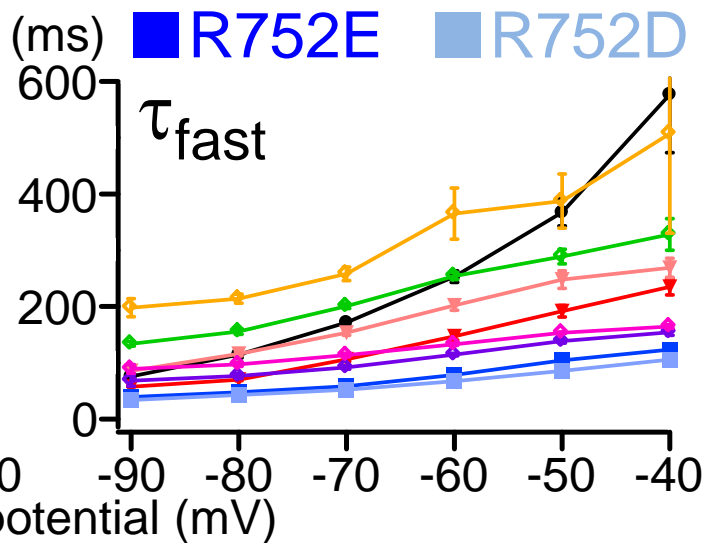
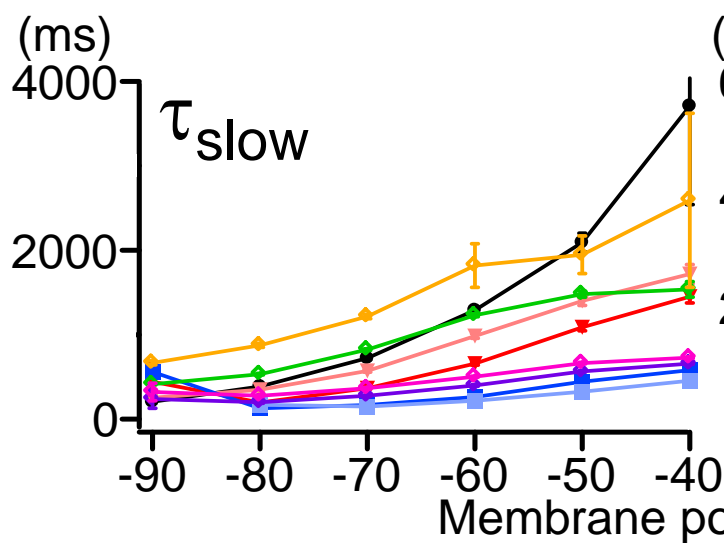
◇ D727R&amp;R752E



◇ D727R&amp;R752D

0.2  $\mu$ A

1 s

**B**

▼ D727K

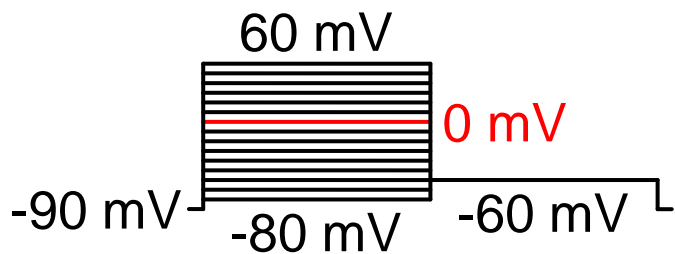
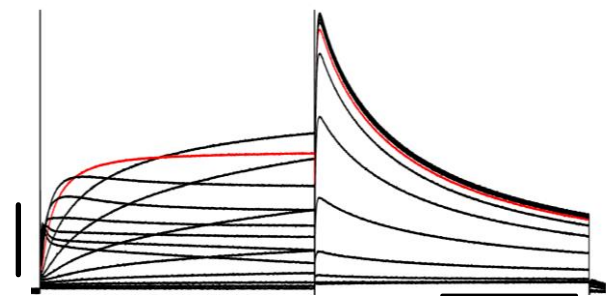
▼ D727R

■ R752E

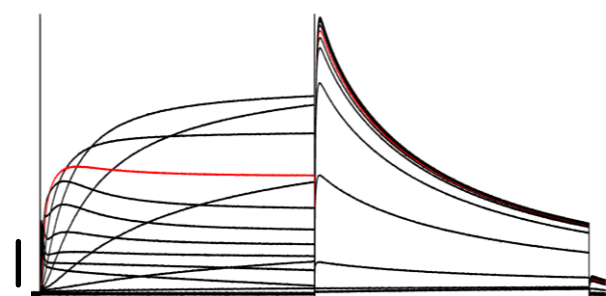
■ R752D

**A**

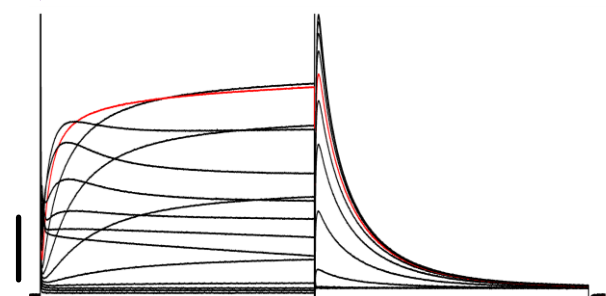
● WT



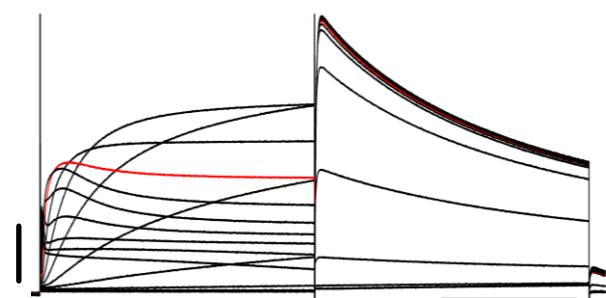
◇ D727K&R752E



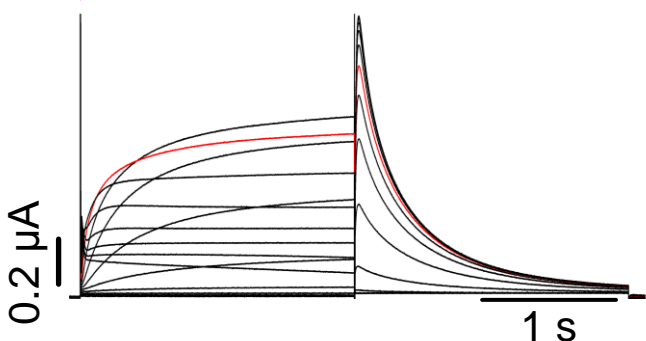
◇ D727K&R752D



◇ D727R&R752E



◇ D727R&R752D



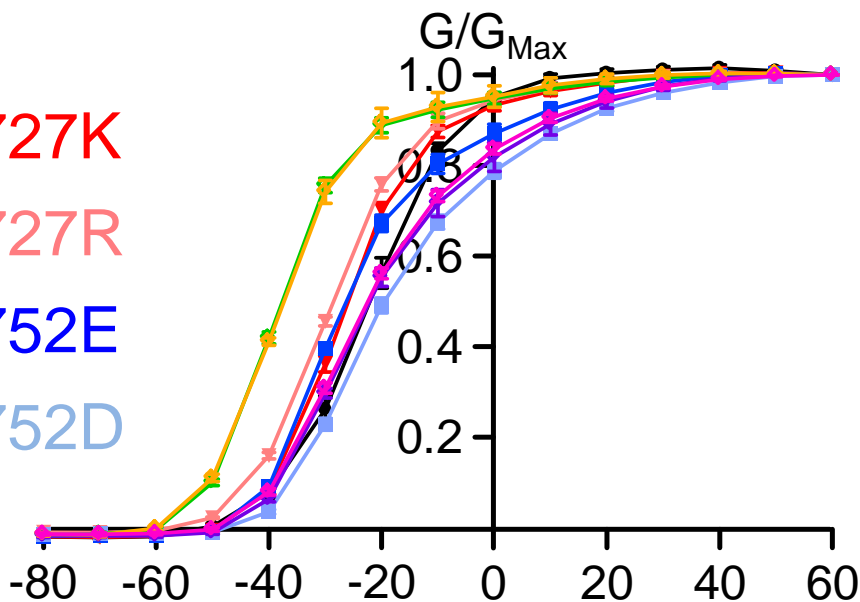
**B**

▼ D727K

▼ D727R

■ R752E

■ R752D



$V_{1/2}$  (mV)

● :  $-22.3 \pm 1.2$

▼ :  $-26.3 \pm 0.6$

▼ :  $-28.9 \pm 0.4$

■ :  $-26.2 \pm 0.7$

■ :  $-18.9 \pm 0.8$

◇ :  $-38.1 \pm 0.5$

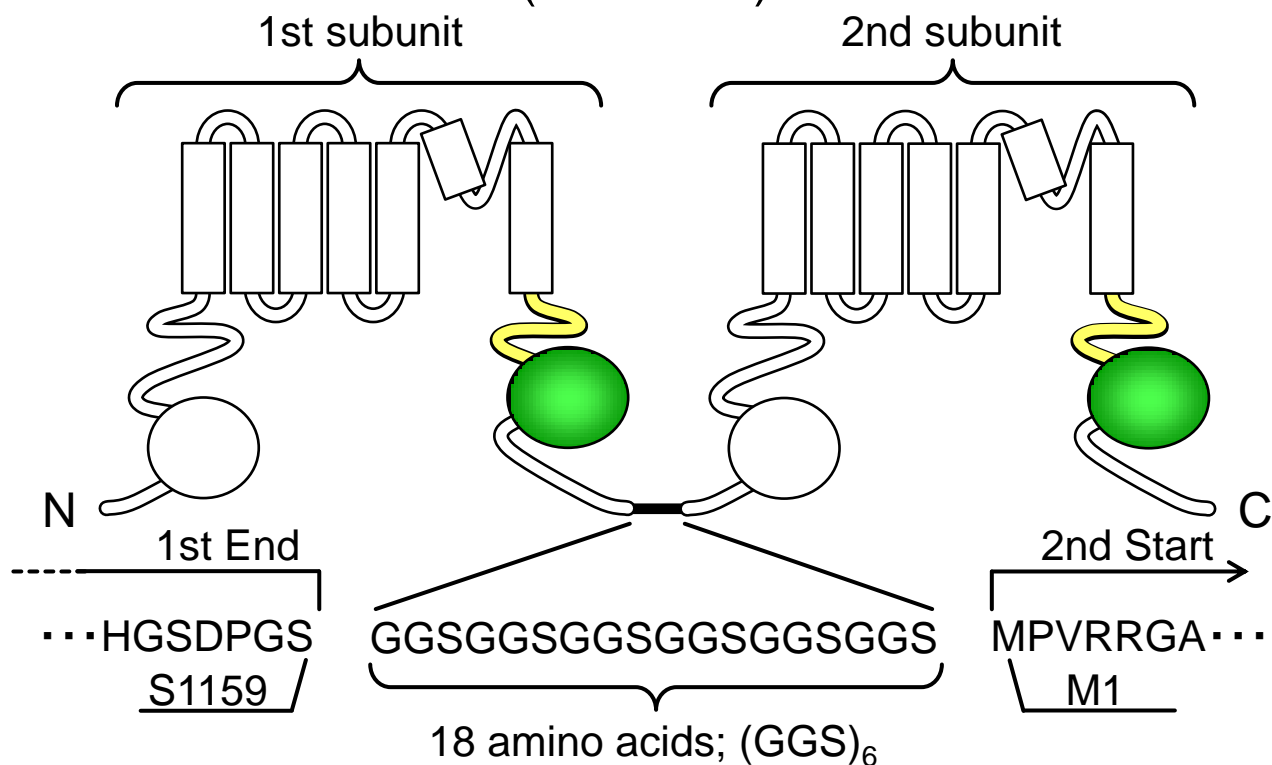
◇ :  $-21.5 \pm 1.1$

◇ :  $-37.8 \pm 0.3$

◇ :  $-22.4 \pm 0.5$

**A**

Tandem construct (WT---WT)



**B**

	If interaction is "inter" subunit				If interaction is "intra" subunit			
	Intact	Artificial	Sum		Intact	Artificial	Sum	
①	2	2	4		0	0	0	
②	0	0	0		2	2	4	
③	0	4	4		0	4	4	

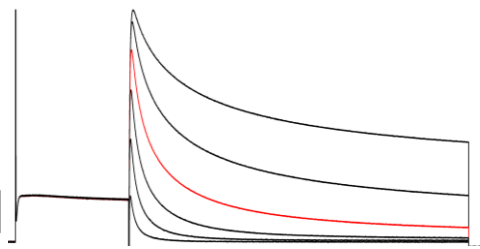
① : Mutation A --- Mutation B (A---B)

② : Mutation A & Mutation B --- WT (A&B---WT)

③ : Mutation A & Mutation B --- Mutation A & Mutation B (A&B---A&B)

**A**

● WT---WT



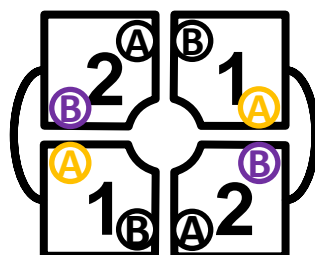
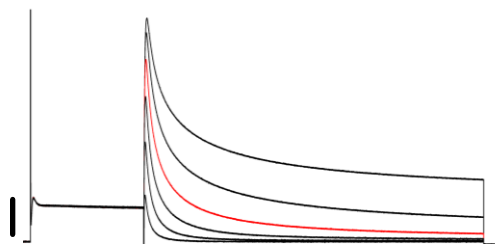
40 mV

-40 mV

-60 mV

-90 mV

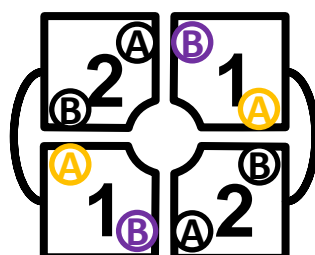
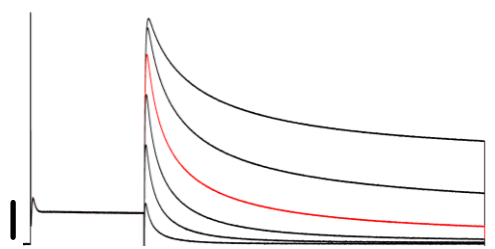
▲ R696E---D767K



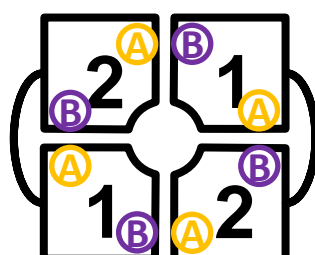
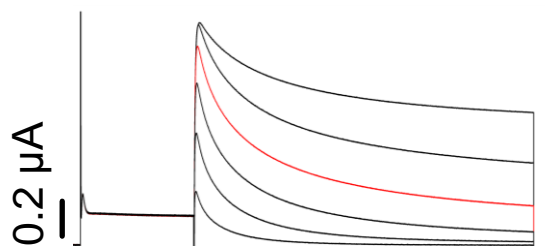
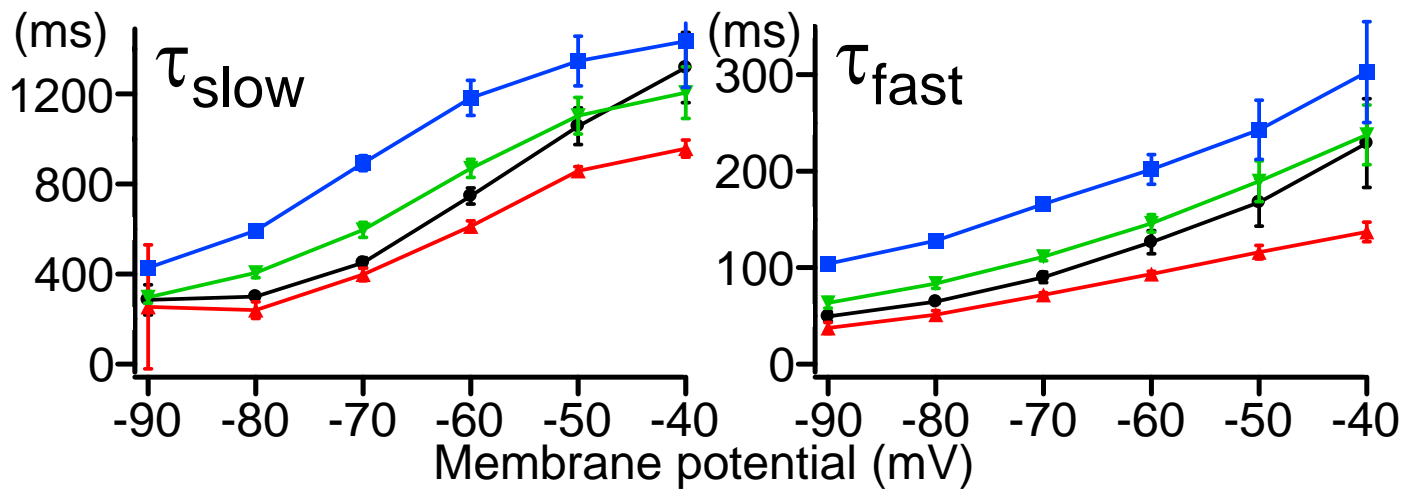
R696E : (A)

D767K : (B)

▼ R696E&amp;D767K---WT

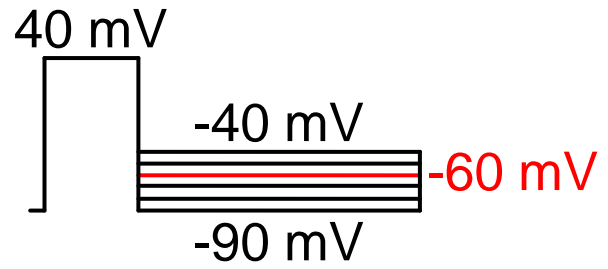
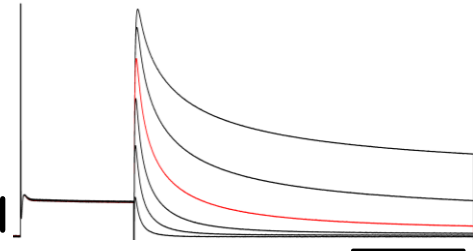


■ R696E&amp;D767K---R696E&amp;D767K

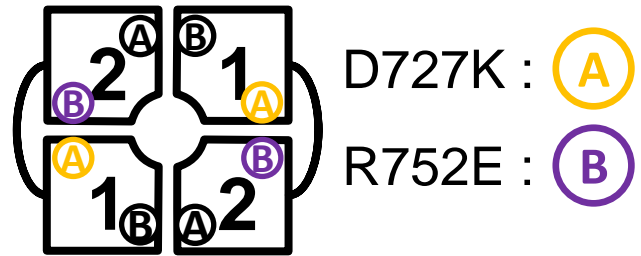
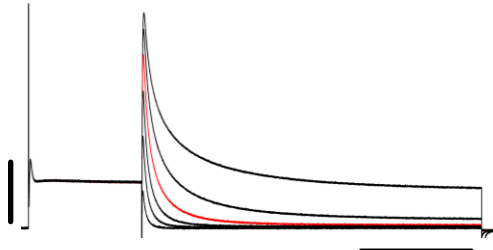
**B**

**A**

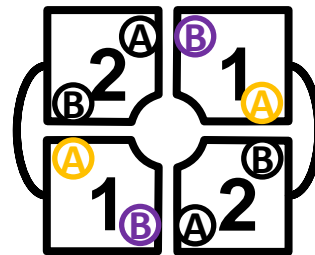
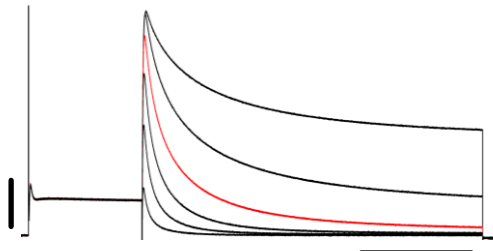
● WT---WT



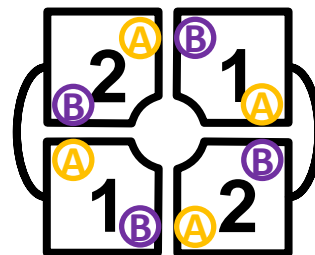
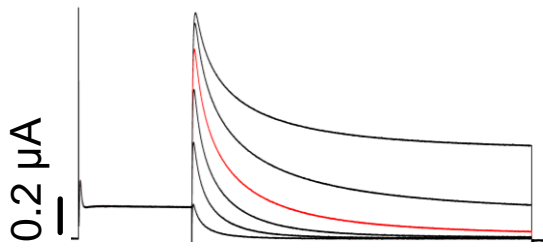
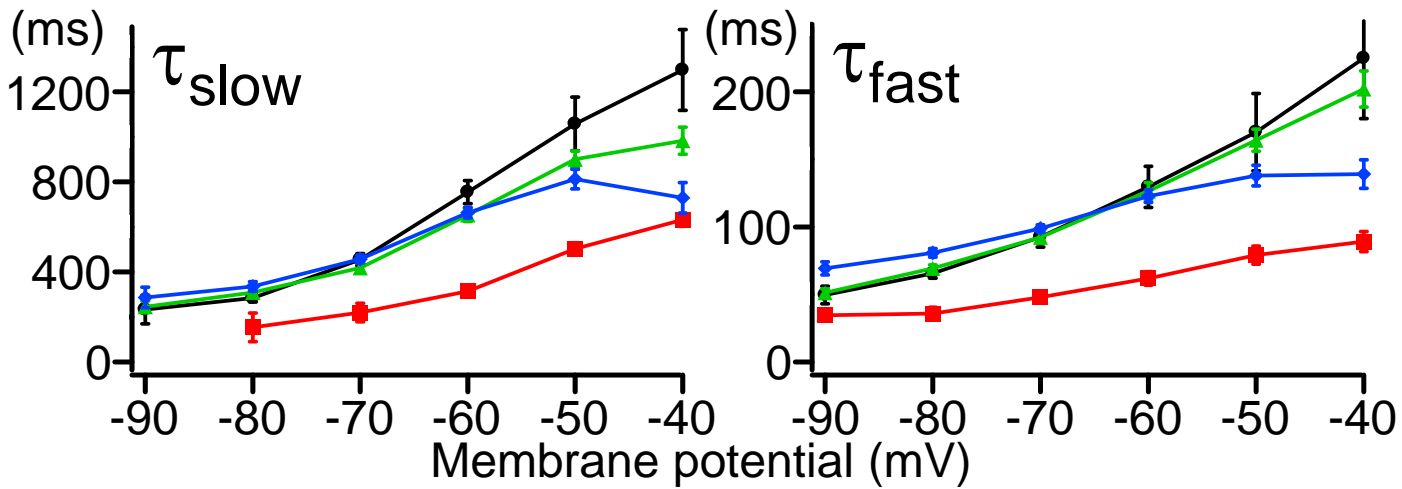
▲ D727K---R752E

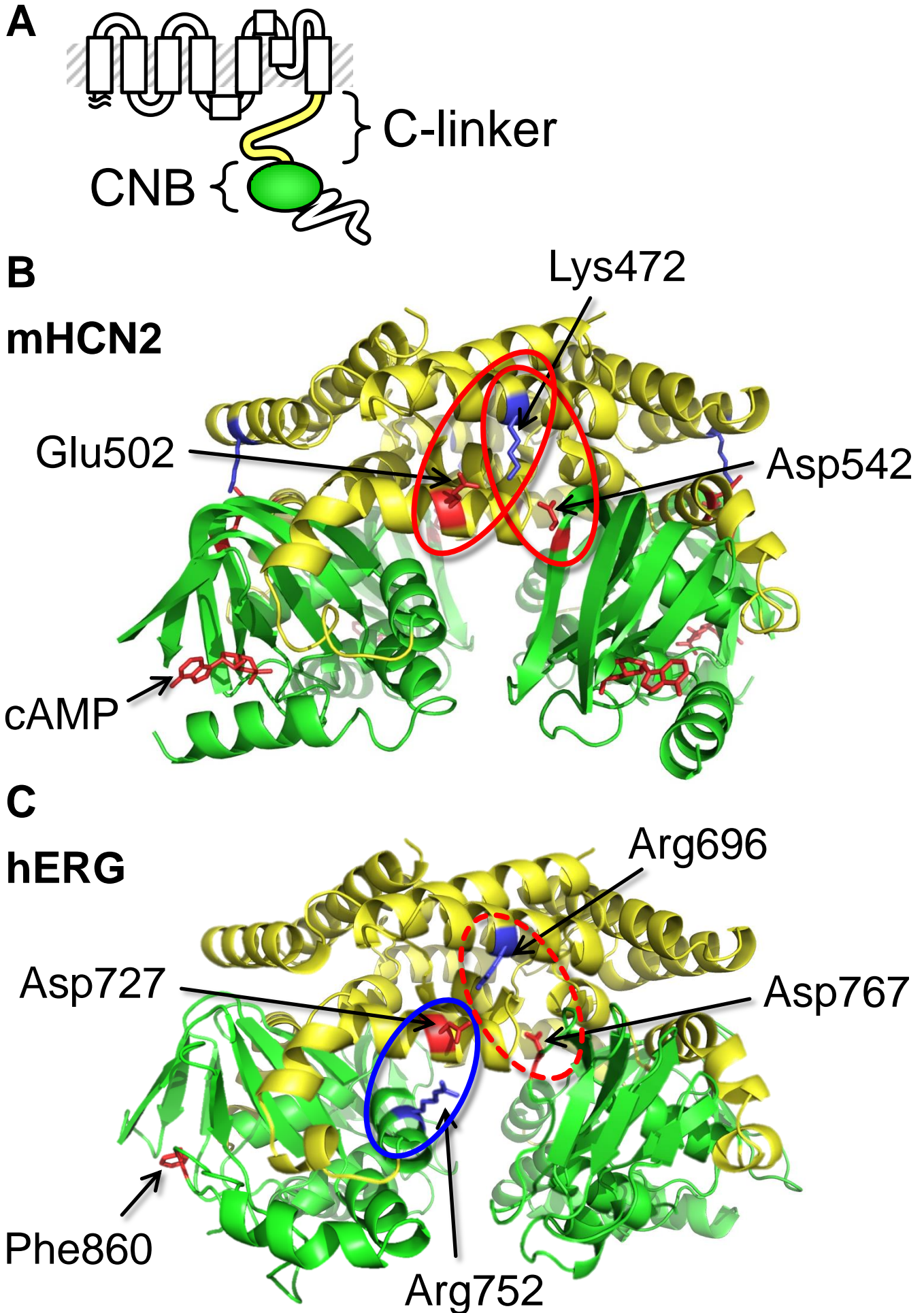


▼ D727K&amp;R752E---WT



■ D727K&amp;R752E---D727K&amp;R752E

**B**



## **Acknowledgements**

I would like to thank Professor Yoshihiro Kubo for consistent supports, discussions, and encouragements during the entire course of this doctoral thesis work. I also would like to thank Associate professor Koichi Nakajo (Osaka Medical College) for discussions and encouragements throughout first three years. I also would like to thank Associate professor Michihiro Tateyama and Assistant professor Takushi Shimomura for supports, discussions, and encouragements during this work. I also would like to thank all members of Kubo laboratory for technical supports and encouragements during this work. Finally, I would like to thank my parents for supporting and encouraging me throughout my study.